Journal of Physiology (1988), **405**, *pp.* 289–320
With 10 *text-figures*
Printed in Great Britain

THE DYNAMICS OF THE CAT RETINAL Y CELL SUBUNIT

BY JONATHAN D. VICTOR

From the Department of Neurology, Cornell University Medical College, 1300 York Avenue, New York, NY 10021, U.S.A. and Laboratory of Biophysics, The Rockefeller University, 1230 York Avenue, New York, NY 10021, U.S.A.

(*Received 4 August 1987*)

SUMMARY

1. The dynamics of the subunit mechanism of individual cat Y retinal ganglion cells are investigated. In order to isolate the response of the non-linear subunit mechanism, the visual stimuli were sine gratings of a spatial frequency sufficiently high so that contrast reversal of the grating elicited no fundamental response in any spatial phase. For study of the non-linear subunit mechanism, the contrast of the spatial sine grating was varied in time by a temporal modulation signal, consisting of either a square wave or a sum of sinusoids.

2. The responses of twenty-three Y ganglion cells (sixteen on-centre, seven off-centre) to these two stimulus types were measured at a range of contrasts. Responses to the sum-of-sinusoids signal were characterized by the second-order frequency kernel. The overall size of the second-order frequency kernel was approximately proportional to contrast. The deviation from proportionality suggested a power-law scaling, with a power in the range 0·8–0·9.

3. Square-wave responses, as characterized by the post-stimulus histogram, demonstrated identical responses at both reversals of the grating. A similar contrast dependence was observed in the overall size of the square-wave responses.

4. In order to attempt to predict the square-wave responses from the sum-of-sinusoids responses, the second-order frequency kernel measured at each contrast level was fitted with a lumped linear–static non-linear–linear model. In eighteen of twenty-three cells (eleven on-centre, seven off-centre), this model provided an adequate description of the response to the sum-of-sinusoids stimulus. In these cells, the linear–static non-linear–linear model accurately reproduced the square-wave response.

5. In the remaining five ganglion cells (all on-centre), the second-order frequency kernel could not be fitted by a linear–static non-linear–linear model. This diversity of dynamical properties among Y cells was not apparent from the responses of these Y cells to the square-wave temporal stimulus.

6. In the eighteen Y ganglion cells that were fitted well with the linear–static non-linear–linear model, substantial variation of the dynamical parameters was found. However, there were systematic differences between the dynamics of the typical on-centre and off-centre ganglion cells. These differences relate to both linear stages of the model, and are not merely consequences of the lower firing rate of the off-centre cells.

7. In these ganglion cells, the dynamics of the first linear filter were similar to the linear dynamics of the X cell centre. There was a tendency for greater transience in the first linear filter of the Y cell compared with that of the X cell. However, most of the greater transience of the Y cell response originates in the second linear filter. The non-linearity *per se* does not contribute to the transience of the Y cell.

INTRODUCTION

The retinal ganglion cells, the output neurones of the retina, provide an early window onto the organization of visual information into parallel pathways (Lennie, 1980). In the cat, two major categories of ganglion cells may be distinguished on the basis of their receptive-field organization: X cells, with qualitatively linear spatial summation, and Y cells, with dramatically non-linear spatial summation (Enroth-Cugell & Robson, 1966).

Along with the linear/non-linear distinction, other physiological features separate these cell populations: X cell responses are sustained while Y cells are transient (Cleland, Dubin & Levick, 1971). X cell receptive-field centres are much smaller than Y cell receptive-field centres at corresponding retinal locations; this correlates with morphologic differences between dendritic trees of X(β) and Y(α) cells (Boycott & Wässle, 1974). One aim of this paper is to determine the relationship between two of these characteristic physiological features of the Y cell: non-linearity and transience.

Another salient feature of the organization of the cat retina is that X and Y cells share input from the same bipolar cells (McGuire, Stevens & Sterling, 1984). Thus, although the X/Y distinction is present at the ganglion cell level, it appears to lack a morphological or physiological correlate at the bipolar cell level.

Qualitative features of the Y cell non-linear response imply that it is generated by a network of subunits, each of which sums light linearly before applying a non-linear transduction (Hochstein & Shapley, 1976*b*; Victor & Shapley, 1979). These studies suggested that the bipolar cell is the anatomical correlate of the Y cell subunit, as well as the main input along the linear pathway to the X cell. This motivates the second aim of this paper: a comparison of Y cell subunit dynamics with those of the X cell.

The overall experimental strategy of this study is to isolate the non-linear subunit contribution to the Y cell response, and to use two different temporal modulation signals to probe its dynamics. The non-linear response may be isolated by stimulation with a spatial grating of high spatial frequency (Hochstein & Shapley, 1976*a*). As probes of subunit dynamics, we use temporal modulation signals consisting of either a sum of sinusoids or a square wave. The sum of sinusoids is a broad-band, complex signal. It has mathematical properties that make it an efficient tool for collecting data suitable for constructing a dynamical model. The square-wave signal provides a means to test the dynamical model and facilitates comparison with more traditional studies of ganglion cell properties.

With a concise dynamical model in hand, we can mathematically dissect the Y cell non-linear pathway, and compare its properties with those of the X cell centre (Victor, 1987). This comparison indicates that the more transient nature of the Y cell

response is due primarily to a second stage of linear processing following the non-linearity, and not to the non-linearity itself. Furthermore, the dynamics of the non-linear pathway of on-centre and off-centre Y cells are distinct; this is in contrast to the similarity of the linear pathways of on- and off-centre X cells.

METHODS

Physiological methods

Recordings of single retinal ganglion cell activity were made in fourteen adult male and female cats, including six cats used in the companion study of X cells (Victor, 1987). The physiological preparation was identical to that of the X cell study, and will only be summarized here.

Anaesthesia was induced with ketamine (10 mg/kg I.M.) and maintained during surgery with sodium thiamylal administered I.V. as needed. During recording, anaesthesia was maintained with urethane (0·2 g/kg I.V., loading; 0·1 g kg^{-1} 24 h^{-1} I.V., maintenance) and paralysis was induced with gallamine triethiodide (5 mg kg^{-1} h^{-1} I.V.). During paralysis, depth of anaesthesia was monitored by blood pressure, heart rate, EEG, and salivation. Blood pressure was maintained above 90 mmHg with fluids if needed; end-expiratory CO_2 was maintained in the range 3·0–3·5%, and temperature was maintained at 38–39 °C. Glucose and oxygen were administered periodically. The corneas, protected with contact lenses with a 3 mm diameter artificial pupil, were lavaged periodically with saline.

Ringer solution-filled pipette microelectrodes (typical resistance, 10–30 MΩ) were used to record single-unit activity of retinal ganglion cells, either as axon spikes in the optic tract, or as unitary S-potential activity in the dorsal lateral geniculate nucleus (Kaplan & Shapley, 1984). The receptive field of the unit was mapped on a tangent screen, and the unit was classified as X or Y by its response to a high spatial frequency grating (Hochstein & Shapley, 1976*a*). Refraction was corrected by trial lenses chosen to optimize the unit's response to fine patterns. We determined two quantities – the centre spatial frequency resolution and the subunit spatial frequency resolution – by listening to the response of the unit to gratings at a contrast of 0·5. The centre spatial frequency resolution was defined as the spatial frequency of the finest grating which elicited a detectable linear (bar-for-bar) response to a drifting grating, moving at a velocity of 2 bars/s. The subunit spatial frequency resolution was defined as the spatial frequency of the finest grating which elicited a frequency-doubled response to square-wave contrast reversal at 2 Hz. For quantitative study, a discriminator circuit was set to send pulses to the computer at each occurrence of an action potential of the isolated unit. The number of impulses during each frame of the display (3·699 ms) was recorded on-line by a PDP 11/23 computer for subsequent analysis. Off-line analysis (plotting, kernel computation, and modelling) was performed on a PDP 11/73 computer.

Stimulus description

Visual stimuli were realized on a Tektronix 608 display oscilloscope with a fast white (P4) phosphor. The *X* (horizontal), *Y* (vertical) and *Z* (intensity) voltages were generated by specialized electronics (Milkman, Schick, Rossetto, Ratliff, Shapley & Victor, 1980) interfaced to the PDP 11/23 computer which recorded impulse arrivals. This apparatus provided for control of a 256 × 256 pixel raster display at a frame rate of 270·3 Hz. The raster has a mean luminance of 100 cd/m^2, with the *Z* input of the oscilloscope modified so that luminance is linear as a function of voltage for variations around the mean of up to 50%.

Each visual stimulus consisted of a stationary pattern whose contrast varied in time. In most of the experiments, the pattern was a spatial sine grating whose spatial frequency was chosen to be half of the subunit spatial frequency resolution of the cell under study. In some Y cells, the centre spatial frequency resolution was sufficiently high so that this grating elicited a linear response as well; in these units, a higher spatial frequency (typically 75% of the subunit spatial frequency resolution) was used.

Data collection was segmented into a sequence of 35 s episodes. The first 5 s of the response to each stimulus pattern were discarded; the remaining 30·3 s (8192 frames) comprise the data saved for later study. Episodes were of two types: 'analysis' and 'synthesis'. The analysis episodes provided data from which model parameters were determined; the synthesis episodes provided

measurements of responses to unrelated temporal patterns and provided for testing of the model.

In all episodes, the average luminance over both space and time was a constant value $L_0 = 100$ cd/m^2. The fractional deviation from this mean luminance (the signed Weber fraction) was equal to a product of a fixed spatial function (a sine grating, denoted $q(X, Y)$) and a temporal modulation signal $s(t)$. Thus, the luminance $L(X, Y, t)$ of the stimulus at a point (X, Y) and time t is given by

$$L(X, Y, t) = L_0[1 + s(t)\, q(X\, Y)]. \tag{1}$$

The temporal modulation signal $s(t)$ is either an analysis signal $s_{\text{ana}}(t)$ or a synthesis signal $s_{\text{syn}}(t)$, as described below. The maximum excursion of the spatial function $q(X, Y)$ was equal to 1, and was always over the receptive-field centre (by convention at $(X, Y) = (0, 0)$). That is, a grating of spatial frequency k was specified by the spatial function $q(X, Y) = \cos(2\pi kX)$.

The models which will be developed below have the (signed) Weber fraction as their input. For all stimuli used in these studies, the (spatial) average of the spatial function $q(X, Y)$ was zero, as was the (temporal) average of the modulation signal $s(t)$. Thus, the signed Weber fraction at the receptive-field centre is always equal to the temporal modulation signal $s(t)$.

The temporal modulation signal for the analysis episodes was a sum of sinusoids at eight nearly incommensurate frequencies f_j. For each modulation depth m_{ana}, eight sum-of-sinusoids signals were constructed with distinct relative phases of the component sinusoids. These eight distinct analysis signals are denoted $s_{\text{ana},\,p}(t)$ $(p = 1, 2, \ldots, 8)$. They are defined by

$$s_{\text{ana},\,p}(t) = m_{\text{ana}} \sum_{j=1}^{8} \cos(2\pi f_j t + \phi_{j,\,p}). \tag{2}$$

In this equation, m_{ana} is the modulation depth produced by each sinusoidal component. The eight frequencies f_j are approximately equally spaced logarithmically: 0·231, 0·495, 1·023, 2·079, 4·191, 8·415, 16·863 and 33·758 Hz. These frequencies are exact integer multiples (7, 15, 31. 63, 127, 255, 511, 1023) of the common fundamental frequency 0·032999 Hz. The phases $\phi_{j,p}$ are all $+\pi/2$ or $-\pi/2$, as determined by the elements of an eight-by-eight Hadamard matrix (Table A1 of Victor & Shapley, 1980). The analysis signal was presented with modulation depths per sinusoid m_{ana} of 0·0156, 0·0312, 0·0625 and 0·125. The root-mean-squared modulation depth of the sum-of-sinusoids signal is $2m_{\text{ana}}$; the maximum modulation depth, which is achieved only once in 65536 bins, is $8m_{\text{ana}}$.

In the synthesis episodes, the temporal modulation signal $s_{\text{syn}}(t)$ consisted of a symmetrical square-wave signal, of temporal frequency $f_{\text{syn}} = 1{\cdot}05$ Hz, with equal excursion above and below zero:

$$s_{\text{syn}}(t) = m_{\text{syn}}\, sq(f_{\text{syn}}\, t), \tag{3}$$

where $m_{\text{syn}}(t)$ is the modulation depth of the synthesis episode and $sq(u)$ is a symmetrical square wave function defined by

$$sq(u) = \begin{cases} +1, \text{ if } n \leqslant u < n+\frac{1}{2} & \text{for some integer } n \\ -1, \text{ if } n+\frac{1}{2} \leqslant u < n+1 & \text{for some integer } n. \end{cases} \tag{4}$$

The square-wave synthesis episodes were run at a range of modulation depths m_{syn} (typically 0·125, 0·25 and 0·5).

Analysis and synthesis episodes were alternated, with 10 s between episodes during which the display was a uniform field at the mean luminance. Modulation depths were increased by a factor of two after each analysis–synthesis pair. A block consisted of one episode of each condition at each modulation depth. This block was repeated eight times; the phase ($\phi_{j,p}$ of eqn (2)) of the input sinusoid for frequency j on repetition p was chosen as described above. This procedure provides for accurate measurement of the first- and second-order frequency kernels, without interference from higher-order combination frequencies below order eight (Victor & Shapley, 1980).

Analytical methods

Responses to the square-wave stimuli $s_{\text{syn}}(t)$ were described by the standard post-stimulus time histogram. Each histogram was derived from eight records of 30·3 s, each of which contained 32 cycles of the 1·05 Hz square wave. The bin width for the histograms was one frame of the display, of 3·699 ms.

Responses to the sum-of-sines stimuli $s_{\text{ana},p}(t)$ were used to calculate the frequency kernels (Victor & Shapley, 1980). The frequency kernels generalize the notion of a transfer function to non-linear transducers. The frequency kernels are obtained from the Fourier components of the transducer's response. The first-order frequency kernel at frequency f_j and modulation depth m_{ana}, denoted $K_1(f_j;m_{\text{ana}})$, is proportional to the Fourier component of the response at the input frequency f_j. The second-order frequency kernel $K_2(\pm f_j,f_k;m_{\text{ana}})$ at a pair of input frequencies $(\pm f_j,f_k)$ is proportional to the Fourier component of the response at the combination frequency $\pm f_j,f_k$.

For the analysis of impulse trains, the unit's response $r_{\text{ana},p}(t)$ to the stimulus $s_{\text{ana},p}(t)$ is taken to be a train of δ-functions, one at the time of occurrence of each impulse. The first-order frequency kernel is defined by

$$K_1(f_j;m_{\text{ana}}) = 2\langle r_{\text{ana},p}(t)\exp[-\iota(2\pi f_j t+\phi_{j,p})]\rangle. \tag{5}$$

The second-order kernel is defined by

$$K_2(f_j,f_k;m_{\text{ana}}) = 2\langle r_{\text{ana},p}(t)\exp[-\iota(2\pi f_j t+2\pi f_k t+\phi_{j,p}+\phi_{k,p})]\rangle \quad (j\neq k),$$

$$K_2(-f_j,f_k;m_{\text{ana}}) = 2\langle r_{\text{ana},p}(t)\exp[-\iota(-2\pi f_j t+2\pi f_k t-\phi_{j,p}+\phi_{k,p})]\rangle \quad (j\neq k),$$

and

$$K_2(f_j,f_j;m_{\text{ana}}) = 4\langle r_{\text{ana},p}(t)\exp[-\iota(4\pi f_j t+2\phi_{j,p})]\rangle. \tag{6}$$

In eqns (5) and (6), $\langle\,\rangle$ denotes an average over time t and phase set p, and $\iota=\sqrt{-1}$. The explicit inclusion of phase terms in the averages of eqns (5) and (6) prevents cancellation of responses as they are averaged across distinct phase sets. Because the response $r_{\text{ana},p}(t)$ is considered to be a sum of δ-functions, this average reduces to a trigonometric sum, with one term for each nerve impulse. Note that the frequency kernels have dimensions of impulses/s, and are not normalized for input modulation depth. The frequency kernels, and their relationship to the Wiener kernels, are described more fully elsewhere (Victor & Knight, 1979).

For a non-linear transducer, the first-order frequency kernel is the set of values of the transfer function of the closest-approximating linear transducer at each of the input frequencies, scaled by the modulation depth m_{ana}. The second-order frequency kernel describes the deviation from linearity as measured by interactions of pairs of input sinusoids. The second-order frequency kernel does not furnish a complete description of a non-linear transduction (which would in general require knowledge of kernels of all orders), but does provide a convenient starting point for such a description.

RESULTS

The first step in the present analysis of the Y cell subunit dynamics is the construction of a model. The construction of a model is necessary for two reasons. First, although the second-order frequency kernel (eqn (6)) expresses deviations from linearity, it is not an exhaustive description of such deviations. Without additional information or suppositions as formalized in a model, the second-order frequency kernel is an incomplete description of the subunit dynamics. The second reason for constructing a model is to reduce the amount of data contained in the second-order frequency kernel to a smaller number of parameters. In formulating the model, the sixty-four amplitudes and phases of the second-order frequency kernel (eqn (6)) will be reduced to a much smaller number of dynamical parameters (such as time constants and feed-back strengths) which have a more intuitive physiological meaning.

After the model is constructed, we will check its validity by using the model to predict responses to the square-wave (synthesis) test input (eqn (3)). Then, the model parameters will serve as a basis for the comparison of the dynamics of on- and off-centre cells, and of X and Y cells.

Construction of a dynamical model

As reported in previous studies (Victor & Shapley, 1979), the response of a Y cell to sum-of-sines modulation of a high spatial frequency grating is described by a first-order frequency kernel which is not significantly different from zero (Fig. 1), and a large second-order frequency kernel (Fig. 2*A*). This implies the presence of an even-order non-linearity. Under the conditions of the present study, all Y cells showed the near-absence of the first-order frequency kernel; for this reason, the first-order frequency kernel will be discussed no further.

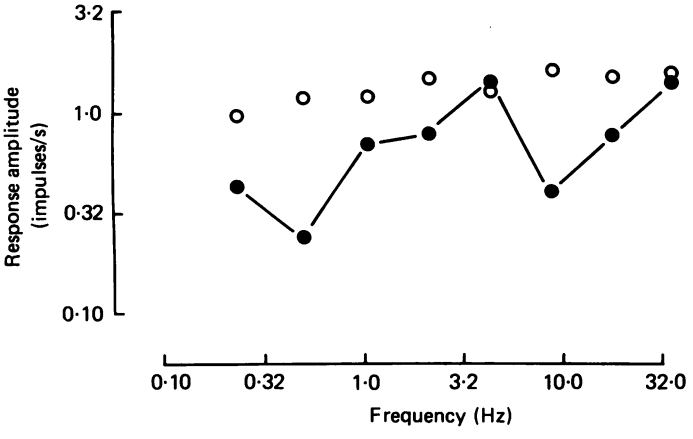

Fig. 1. Amplitudes of the first-order frequency kernel (eqn (5)) of the response of an on-centre Y cell to a 2·0 cycle/deg grating modulated by a sum-of-sinusoids signal with a modulation depth per sinusoid $m_{ana} = 0{\cdot}125$. First-order kernel amplitudes (●) are typically smaller than the uncertainty of measurement, as quantified by the standard deviation of the estimates of the kernel from eight successive episodes (○). Unit 7/6.

Fig. 2. *A*, second-order frequency kernel (eqn (6)) of the response of an on-centre Y cell to a grating modulated by a sum-of-sinusoids signal. These data are derived from the same experiment as Fig. 1. *B*, values of model second-order frequency kernel, derived from eqn (10). Parameters: $M_0 = 46{\cdot}4$, $A_0 b_2(\alpha) = 1201$, $N_{L,U} = 8$, $N_{L,U} T_{L,U} = 56{\cdot}9$ ms, $H_{S,U} = 0{\cdot}757$, $T_{S,U} = 0{\cdot}071$ s, $N_{L,W} = 8$, $N_{L,W} T_{L,W} = 3{\cdot}6$ ms, $H_{S,W} = 0{\cdot}985$, $T_{S,W} = 0{\cdot}032$ s, $D = 2$ ms. *C*, difference between measured (*A*) and model (*B*) second-order frequency kernels. In all panels, the quantity plotted (the frequency kernel or the difference of two frequency kernels) is a complex-valued function of two frequencies. Amplitudes of this function are plotted as a contour map, on a scale of one contour line for 1 impulse/s. The tickmarks point downhill. Phases of this quantity are represented as colour, with green indicating a phase of zero, red indicating a phase shift of one-half a cycle, blue a phase lag of one-quarter cycle, and yellow a phase lead of one-quarter cycle. Thus, real-valued quantities appear with a colour along the red–green line, and imaginary-valued quantities appear with a colour along the blue–yellow line. The surface is interpolated by a cubic spline across the lattice of points $(\pm f_j, f_k)$ on which its value was determined by eqn (6). The upper half of each plot shows values at the sum frequencies $K_2(F_1, F_2)$; the lower half of each plot shows values at the difference frequencies $K_2(-F_1, F_2)$. In each half of the contour map, frequency axes are logarithmically transformed between the lowest test frequency (0·231 Hz) and the highest test frequency (33·758 Hz).

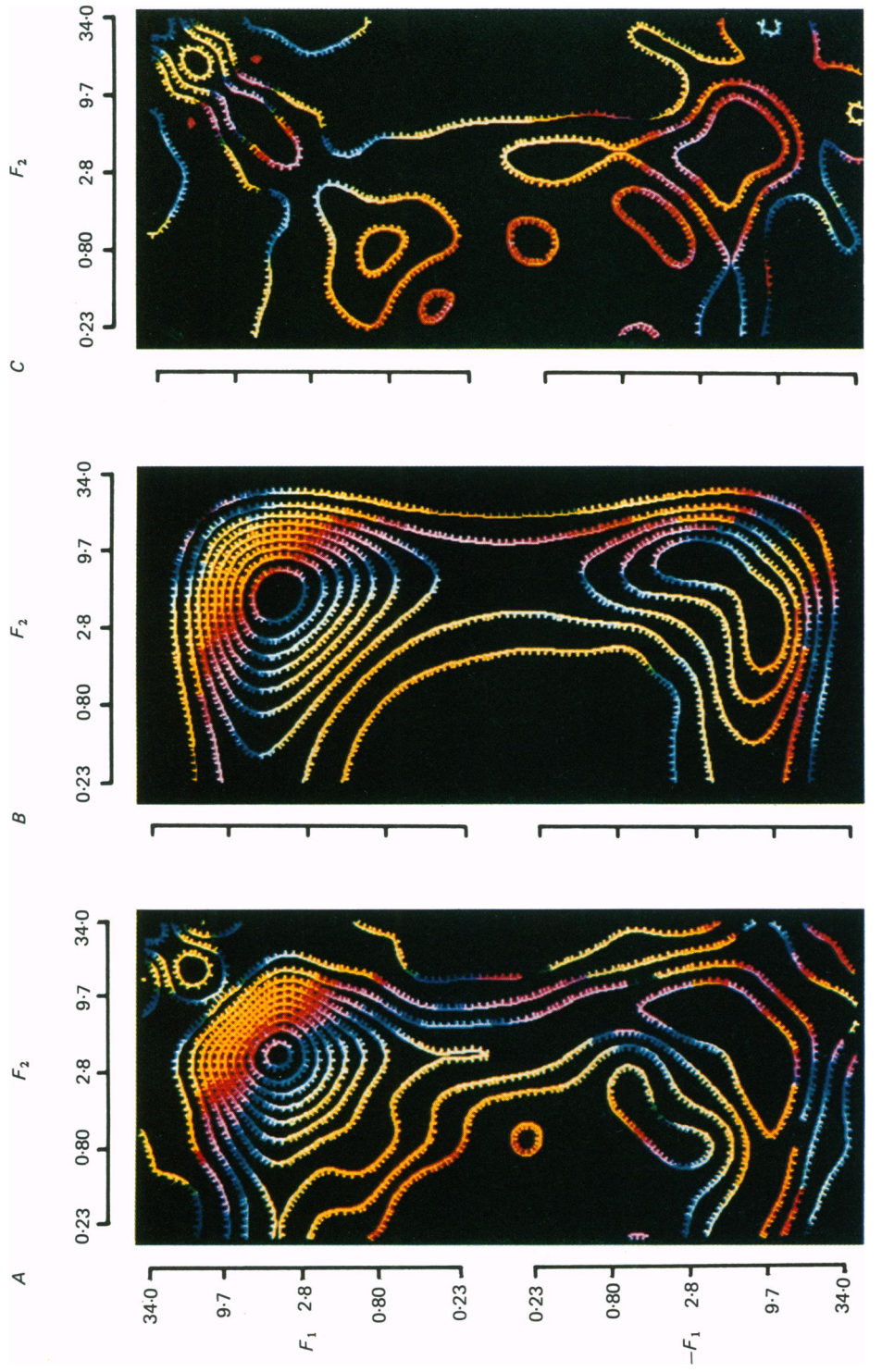
A
B
C
F_2
0·23
0·80
2·8
9·7
34·0
F_1
$-F_1$

TABLE 1. The dynamical model

	Time domain (non-linear)	Frequency domain (linearized)
	First linear filter (U)	
(U)	$u(t) = \int_0^\infty s(t-t')U(t')\,dt'$	$\tilde{u}(\omega) = \tilde{U}(\omega)\,\tilde{s}(\omega)$
		where $\tilde{U}(\omega) = \left(\frac{1}{1+\iota\omega T_{L,U}}\right)^{N_{L,U}} \left(1-\frac{H_{S,U}}{1+\iota\omega T_{S,U}}\right)^{N_{S,U}}$
	Static non-linearity (N)	
(N)	$u'(t) = \lvert u(t)\rvert^\alpha$	
	Second linear filter (W)	
(W)	$w(t) = \int_0^\infty u'(t-t')W(t')\,dt'$	$\tilde{w}(\omega) = \tilde{W}(\omega)\,\tilde{u}'(\omega)$
		where $\tilde{W}(\omega) = \left(\frac{1}{1+\iota\omega T_{L,W}}\right)^{N_{L,W}} \left(1-\frac{H_{S,W}}{1+\iota\omega T_{S,W}}\right)^{N_{S,W}}$
	Impulse generation (I)	
(I)	$r(t) = \max\{A_0\,w(t-D)+M_0, 0\}$	$\tilde{r}(\omega) = A_0\,e^{-\iota\omega D}\tilde{w}(\omega)+M_0\,\delta(\omega)$

Summary of a non-linear model for the dynamics of the Y cell subunit. The model is a sandwich of a static non-linearity between two linear filters. The input to the model is $s(t)$, the signed Weber contrast at the centre. The first linear filter, U, consists of a low-pass filter comprised of $N_{L,U}$ stages of time constant $T_{L,U}$, and a subtractive high-pass filter of strength $H_{S,U}$ and time constant $T_{S,U}$. Its operation is represented in the frequency domain by multiplication by its transfer function $\tilde{U}(\omega)$, and in the time domain by convolution with its impulse response $U(t)$. $U(t)$ is the inverse Fourier transform of $\tilde{U}(\omega)$. The output of the first linear filter, $u(t)$, is the input to a static non-linearity N. This non-linearity is a rectifier with input and output related by a power-law transformation of exponent α. The output of the rectifier, $u'(t)$, is the input to a second linear filter, W. The second linear filter, W, contains a low-pass filter comprised of $N_{L,W}$ stages of time constant $T_{L,W}$, and a subtractive high-pass filter of strength $H_{S,W}$ and time constant $T_{S,W}$. Its operation is represented in the frequency domain by multiplication by its transfer function $\tilde{W}(\omega)$, and in the time domain by convolution with its impulse response $W(t)$. $W(t)$ is the inverse Fourier transform of $\tilde{W}(\omega)$. The firing rate $r(t)$ is equal to the output of the second linear stage, $w(t)$, scaled by an overall gain A_0, and added to the firing rate in the absence of stimulation, M_0. It is delayed by a conduction delay D and must be non-negative. The Fourier transforms of $r(t)$, $s(t)$, $u(t)$, $u'(t)$, and $w(t)$ are denoted by $\tilde{r}(\omega)$, $\tilde{s}(\omega)$ $\tilde{u}(\omega)$, $\tilde{u}'(\omega)$, and $\tilde{w}(\omega)$. Note that the static non-linearity is not readily represented in the frequency domain, and the frequency domain representation also neglects the truncation at zero impulses/s.

The qualitative features of the second-order frequency kernel imply a minimal framework for a dynamical model, consisting of a linear filter, followed by a static (instantaneous) non-linearity, followed by a second linear filter. The first linear filter corresponds to processing within an individual subunit; the second linear filter corresponds to pooling of subunit outputs (Table 1 and Fig. 3).

Perhaps the simplest way to embed this concept into a non-linear model is to assume that the non-linearity is quadratic. This is equivalent to the assumption that the higher-order frequency kernels (and the higher-order Wiener kernels) are zero. However, a quadratic non-linearity would imply that overall response size should scale quadratically with contrast, which stands in contradiction to the observed proportional scaling (Hochstein & Shapley, 1976*b*). Not surprisingly (see below), the quadratic assumption will lead to a very poor prediction of the square-wave response.

The approximate proportionality of the response size and contrast suggests that a rectifier is the generator of the non-linearity. Such non-linearities will generate non-

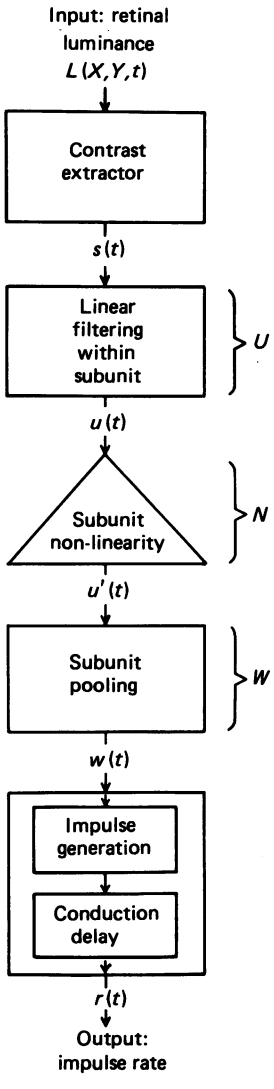

Fig. 3. A diagram of the basic linear–non-linear–linear sandwich model. Components of the model are described in detail in the text and in Table 1.

zero frequency kernels of higher even order. The second-order frequency kernel, together with the assumption that the only non-linearity is rectification, does not suffice to determine these higher-order kernels, or the non-linear model, completely. This is because any network of linear filters and rectifiers combined in series, parallel, and feed-back loops will result in a transducer whose output is proportional to its input; these networks may not be readily distinguishable by their second-order kernels. However, among all such combinations, the linear–non-linear–linear cascade is the simplest.

The linear–non-linear–linear cascade model is diagrammed in Fig. 3. The initial

stage of the model has as its input the stimulus luminance $L(X, Y, t)$ (eqn (1)). A Weber's-law mechanism extracts the signed Weber fraction $s(t)$ from the luminance. (For stimuli used in the present study, the signed Weber fraction $s(t)$ is related to the local luminance fluctuation by a proportionality L_0 (eqn (1).) The rationale for explicitly postulating a Weber's-law mechanism is based on physiological evidence for such a mechanism at the level of the photoreceptor (Baylor & Hodgkin, 1974), and is discussed more fully elsewhere (Victor, 1987). The signed Weber fraction $s(t)$ is operated on by the first linear transducer of the sandwich, denoted U, producing an intermediate signal $u(t)$. In the frequency domain, the intermediate signal $u(t)$ and the signed Weber fraction $s(t)$ are related by multiplication by the transfer function $\tilde{U}(\omega)$ of U:

$$\tilde{u}(\omega) = \tilde{U}(\omega)\,\tilde{s}(\omega). \tag{7}$$

(Here, $\tilde{u}(\omega)$ and $\tilde{s}(\omega)$ denote the Fourier transforms of $u(t)$ and $s(t)$, respectively.) In physiological terms, $u(t)$ represents the retinal signal just prior to the non-linearity of the subunit, and $\tilde{U}(\omega)$ represents the dynamics of the transduction that produces this signal.

The intermediate signal $u(t)$ is the input to a non-linearity N, and the output of the non-linearity is the signal $u'(t)$. Since this non-linearity is assumed to be 'memoryless' or instantaneous, it may be described by

$$u'(t) = N(u(t)). \tag{8}$$

The output of the non-linearity, $u'(t)$, is operated on by the second linear transducer of the sandwich, denoted W. The output of W, denoted $w(t)$, and its input $u'(t)$ are related by multiplication by the transfer function $\tilde{W}(\omega)$ of W:

$$\tilde{w}(\omega) = \tilde{W}(\omega)\tilde{u}'(\omega). \tag{9}$$

In physiological terms, $w(t)$ represents the pooled output of the subunit network, and $\tilde{W}(\omega)$ represents the temporal integration that corresponds to this pooling.

Finally, impulse generation is represented by a process of gain A_0 (with units of impulses/unit contrast), and impulse propagation is represented by a conduction delay D. Other than the addition of a firing rate in the absence of stimulation, denoted M_0, and truncation at 0 impulses/s, the impulse-generation process is assumed to be linear. It is therefore grouped with the filter W, as a linear process which follows the non-linearity.

The formula for the second-order frequency kernel (eqn (6)) for this linear–non-linear–linear sandwich follows from the formula for the Wiener kernel of this transduction (Korenberg, 1973), and the near-identity of the second-order frequency kernel with the Fourier transform of the second-order Wiener kernel (Victor & Knight, 1979). For the linear–non-linear–linear sandwich of Fig. 3, the expected second-order frequency kernel is then approximated by

$$K_2(F_1, F_2; m_{\text{ana}}) = A_0\, b_2(N)\, m_{\text{ana}}^2 \exp[-2\pi\iota(F_1+F_2)D]\, \tilde{U}(2\pi F_1)\, \tilde{U}(2\pi F_2)\, \tilde{W}(2\pi(F_1+F_2)). \tag{10}$$

In this equation, $b_2(N)$ is the coefficient of the second Hermite polynomial in the orthogonal expansion of the defining eqn (8) of the static non-linearity N. This

orthogonal expansion must be performed with respect to a Gaussian of variance equal to the power of $u(t)$. This power, to be denoted P_U, is proportional to the square of the modulation depth m_{ana}:

$$P_U = \tfrac{1}{2} m_{\text{ana}}^2 \sum_{j=1}^{8} |\tilde{U}(2\pi f_j)|^2. \tag{11}$$

As shown in the Appendix, for the power-law rectifier

$$N(u) = |u|^\alpha, \tag{12}$$

the coefficient b_2 of eqn (10) is given by

$$b_2(\alpha) = \alpha\pi^{-\frac{1}{2}} (2P_U)^{\alpha/2-1} \Gamma((\alpha+1)/2) \quad (\alpha \geqslant 0). \tag{13}$$

We are initially concerned with the quadratic ($\alpha = 2$) and linear rectifier ($\alpha = 1$) cases. For these special cases,

$$b_2(2) = 1 \tag{14}$$

and

$$b_2(1) = (2\pi P_U)^{-\frac{1}{2}}. \tag{15}$$

Note that for the quadratic non-linearity ($\alpha = 2$), b_2 (eqn (14)) is independent of the analysis modulation depth m_{ana}, so that the second-order frequency kernel $K_2(F_1, F_2; m_{\text{ana}})$ will be proportional to m_{ana}^2 (eqn (10)). However, for a linear rectifier ($\alpha = 1$), b_2 is inversely proportional to m_{ana} (as seen by substituting eqn (11) into eqn (15)), and thus the second-order frequency kernel will be proportional to m_{ana}^1 (eqn (10)).

In order to apply the model eqn (10) to experimental data, we chose to postulate simple functional forms for the transfer functions $\tilde{U}(\omega)$ and $\tilde{W}(\omega)$. This approach avoids the need for interpolation between measured values of the second-order frequency kernel, and allows direct comparison with X cell dynamics (Victor, 1987). The forms chosen are:

$$\tilde{U}(\omega) = \left(\frac{1}{1+\imath\omega T_{\text{L},U}}\right)^{N_{\text{L},U}} \left(1 - \frac{H_{\text{S},U}}{1+\imath\omega T_{\text{S},U}}\right)^{N_{\text{S},U}} \tag{16}$$

and

$$\tilde{W}(\omega) = \left(\frac{1}{1+\imath\omega T_{\text{L},W}}\right)^{N_{\text{L},W}} \left(1 - \frac{H_{\text{S},W}}{1+\imath\omega T_{\text{S},W}}\right)^{N_{\text{S},W}} \tag{17}$$

Each functional form is thus a product of a series of identical low-pass stages and a series of identical subtractive high-pass stages. In each equation ($* = U$ or W), $T_{\text{L},*}$ is the time constant of each of the $N_{\text{L},*}$ low-pass stages; $H_{\text{S},*}$ is the strength and $T_{\text{S},*}$ is the time constant of each of the $N_{\text{S},*}$ subtractive high-pass stages.

To estimate the parameters of the transfer functions (eqns (16) and (17)), the model second-order frequency kernel (eqn (10)) was fitted to the experimentally determined second-order frequency kernel. The criterion of goodness-of-fit was the

sum of the squares of the deviation of the model from the data, at each of the points of the second-order kernel:

$$R = \sum_{j=1,k=1}^{8} |K_{\text{data}}(f_j,f_k;m_{\text{ana}}) - K_{\text{model}}(f_j,f_k;m_{\text{ana}})|^2 + \sum_{\substack{j=1,k=1 \\ j\neq k}}^{8} |K_{\text{data}}(f_j,-f_k;m_{\text{ana}}) - K_{\text{model}}(f_j,-f_k;m_{\text{ana}})|^2. \quad (18)$$

In this equation, K_{data} is the experimentally determined second-order frequency kernel, and K_{model} is given by the model eqn (10), with $b_2(N)$ set equal to $b_2(\alpha)$ (eqn (13)).

The model parameters were determined by minimizing the residuals (eqn (18)). This minimization formally involves all of the parameters of the filter functions (eqns (16) and (17)), as well as the overall gain A_0, the coefficient $b_2(\alpha)$, and the delay D. The minimization was carried out by an iterative scheme based on the non-linear least-squares algorithm of Fletcher & Powell (1963).

Since the minimization procedure involved a large number of parameters, several special features were exploited to make it more tractable. First, the conduction delay D was not determined by the least-squares procedure, but was calculated from the retinal location according to the data of Stone & Fukuda (1974). Second, the parameters A_0 and $b_2(\alpha)$ were not fitted independently; rather, their product was fitted, and then $b_2(\alpha)$ was determined from eqn (13) based on an assumed value of α.

Third, it was observed that fits to some components of the model were approximately independent. The independence was most apparent with respect to the low-pass stages and the high-pass stages of the model. That is, the value for the low-pass time constants $T_{\text{L},U}$ and $T_{\text{L},W}$ obtained by minimizing the residuals (eqn (18)) with the high-pass parameters held fixed was relatively insensitive to the particular value chosen for the high-pass parameters. This is because $T_{\text{L},U}$ and $T_{\text{L},W}$ affect primarily the rate of roll-off of the frequency kernel at high frequencies, and do not affect the low-frequency amplitudes or phase shifts. This approximate independence enabled the fitting procedure to proceed in an iterative fashion: first, a guess was made for the high-pass parameters, and low-pass time constants were determined by minimization of the residuals (eqn (18)) with the high-pass parameters held fixed, and then the low-pass time constants were held fixed and the high-pass parameters were optimized. In a similar fashion, the high-pass parameters for the first filter ($H_{\text{S},U}$ and $T_{\text{S},U}$) were approximately independent of the high-pass parameters for the second filter ($H_{\text{S},W}$ and $T_{\text{S},W}$); this permitted an iterative approach to fitting the high-pass component. The overall scale factor $A_0 b_2(\alpha)$ interacted strongly with the dynamical parameters, and the low-pass stages of the filters U and W also interacted strongly with each other. When an approximate minimum was located by the iterative procedure outlined above, a final minimization was performed in which all continuous parameters ($A_0 b_2(\alpha)$, $T_{\text{L},U}$, $H_{\text{S},U}$, $T_{\text{S},U}$, $T_{\text{L},W}$, $H_{\text{S},W}$, $T_{\text{S},W}$) were simultaneously allowed to vary.

The above procedure was carried out parametrically for a range of values for the integer parameters $N_{\text{L},U}$, $N_{\text{S},U}$, $N_{\text{L},W}$, and $N_{\text{S},W}$. Again, the low-pass parameters

TABLE 2. Population statistics for model parameters

Parameter	Y cell population	Minimum	Maximum	Median	Mean	S.D.	c.v.	P
$A_0 b_2(\alpha)$ (impulses s^{-1} (unit contrast)$^{-2}$)	On	632	2296	1305	1444	570	0·39	0·024
	Off	207	1670	493	796	608	0·76	
	All	207	2296	1210	1192	654	0·55	
M (impulses/s)	On	41·3	78·9	51·5	55·6	13·1	0·23	< 0·001
	Off	2·3	40·2	12·3	15·2	13·1	0·86	
	All	2·3	78·9	44·5	39·8	23·9	0·60	
$N_{L,U}T_{L,U}$ (ms)	On	34·7	60·5	49·4	47·9	8·3	0·17	0·044
	Off	23·3	54·6	31·9	36·8	11·5	0·26	
	All	23·3	60·5	43·6	43·6	10·9	0·25	
$H_{S,U}$ (dimensionless)	On	0·637	1·424	0·964	1·007	0·302	0·30	> 0·1
	Off	0·694	1·051	0·958	0·884	0·151	0·17	
	All	0·637	1·424	0·964	0·959	0·256	0·27	
$T_{S,U}$ (s)	On	0·041	0·359	0·056	0·088	0·091	1·03	> 0·1
	Off	0·013	0·125	0·074	0·072	0·042	0·58	
	All	0·013	0·359	0·068	0·082	0·074	0·90	
$N_{L,W}T_{L,W}$ (ms)	On	1·7	15·6	8·6	8·0	3·8	0·48	0·006
	Off	6·2	36·9	22·6	20·6	11·9	0·58	
	All	1·7	36·9	9·4	13·0	9·9	0·76	
$H_{S,W}$ (dimensionless)	On	0·452	1·174	0·717	0·801	0·258	0·32	0·02
	Off	0·237	0·670	0·544	0·518	0·155	0·30	
	All	0·237	1·174	0·633	0·691	0·260	0·38	
$T_{S,W}$ (s)	On	0·002	0·045	0·011	0·014	0·012	1·07	0·006
	Off	0·010	0·101	0·046	0·044	0·033	0·75	
	All	0·002	0·101	0·014	0·026	0·026	1·00	

Population statistics for the parameters of a non-linear model for the dynamics of the Y cell subunit. The meaning of the parameters is defined in the text and Table 1. S.D., standard deviation; c.v., coefficient of variation (standard deviation/mean). Probability values for the significance of the difference of means population statistics for on- and off-centre Y cells were calculated by a bootstrap analysis of variance (Efron, 1980). The conduction delay D of Table 1 was in the range 1·0–3·0 ms for all Y cells.

$N_{L,U}$ and $N_{L,W}$ and the high-pass parameters $N_{S,U}$ and $N_{S,W}$ were independent. For all units studied, single-stage high-pass filters ($N_{S,U} = 1$ and $N_{S,W} = 1$) provided the best fits. The optimum number of low-pass stages was more variable, and ranged from six to twenty-four. This variability is probably due to problems in accurate measurement of the parameter, rather than true biological variability. The parameters $N_{L,*}$ govern the slopes of their respective transfer functions at high frequencies. The apparent value of this slope depends on the measured response at f_8, the highest input frequency (33·758 Hz), but responses at this frequency are close to noise. Although the steep high-frequency attenuation of responses implies that the $N_{L,*}$ are large in comparison to 1, this does not determine their values with precision. For values of $N_{L,*} \gg 1$ and for frequencies small in comparison to $1/T_{L,*}$, values of the transfer functions (eqns (16) and (17)) depend primarily on the integration time $N_{L,*}T_{L,*}$. Thus, we focus on the low-pass integration times $N_{L,U}T_{L,U}$ and $N_{L,W}T_{L,W}$ rather than on the individual parameters. This situation is analogous to the analysis of the quasilinear dynamics of the X cell (Shapley & Victor, 1981; Victor, 1987).

To facilitate comparison of the integration time preceding and following the non-linearity, the total number of low-pass stages, $N_{L,U}+N_{L,W}$, was arbitrarily fixed at sixteen, and the individual values of $N_{L,U}$ and $N_{L,W}$ were allowed to assume the values {0, 1, 4, 8, 12, 15, 16}. This procedure provided values for the combinations $N_{L,U}T_{L,U}$ and $N_{L,W}T_{L,W}$ that were similar to those obtained (in two Y cells) by the much more laborious procedure of allowing $N_{L,U}$ and $N_{L,W}$ to vary independently through the range 0–16. For most units, the optimum fit was obtained at $N_{L,U} = 8$, $N_{L,W} = 8$. Four units (two on-centre, two off-centre) were best fitted with $N_{L,U} = 4$, $N_{L,W} = 12$; one off-centre unit was best fitted with $N_{L,U} = 12$, $N_{L,W} = 4$.

The modelling procedure detailed above provided close fits to the observed second-order frequency kernels in eighteen of the twenty-three Y cells studied. In these ganglion cells, deviations of measured values of the second-order frequency kernel and fitted values were typically less than 2 impulses/s, which is comparable to the measurement error. The five ganglion cells that were not well-fitted by the model will be discussed separately below.

An example of the model second-order frequency kernel is shown in Fig. 2*B*, and the difference between the measured and fitted values is shown in Fig. 2*C*. Note that amplitude and phases are both used in calculation of the residuals (eqn (18)) and the difference map of Fig. 2*C*. It is evident that the major qualitative features of the measured second-order kernel (the heights and positions of the peaks) are captured. The typical deviation of experimental and model kernel, which may be quantified by the square root of the average term in the sum (eqn (18)), was 1·4 impulses/s. The greatest deviations occur near the diagonals $F_1 = F_2$ and $F_1 = -F_2$, the regions in which there is the greatest uncertainty in the experimental determination of the second-order frequency kernel (Victor & Shapley, 1980).

The dynamical parameters determined from eighteen on-centre Y cells and seven off-centre Y cells are summarized in Table 2. These data were obtained by the above fitting procedure applied to responses elicited by a sum-of-sinusoids signal (eqn (2)) producing a modulation depth of 0·125 per sinusoid.

Testing the model

One purpose of the modelling procedure developed above was to summarize the dynamics of the Y cell non-linear response in a relatively small number of parameters. However, before we attempt to draw any conclusions from the parametric model, it is necessary to demonstrate that the model does indeed summarize the subunit dynamics. This is a stricter requirement than merely that of correspondence to the second-order kernel: in order to demonstrate that the agreement with the measured second-order kernel is not just a matter of postulating enough parameters, we demonstrate that the model has predictive power.

To do this, we use the above dynamical model to predict the response to modulation signals that are distinct from the sum-of-sinusoids signal used to construct the model. The main test signal that we use for this purpose is the square wave (eqn (3)). The 'transientness' of the step response is thought to be a characteristic feature of the Y cell (Cleland, Dubin & Levick, 1971). The square-wave stimulus is a strong test of the model because it contains many frequencies not present in the sum-of-sinusoids stimulus, and because the stimulus transient may

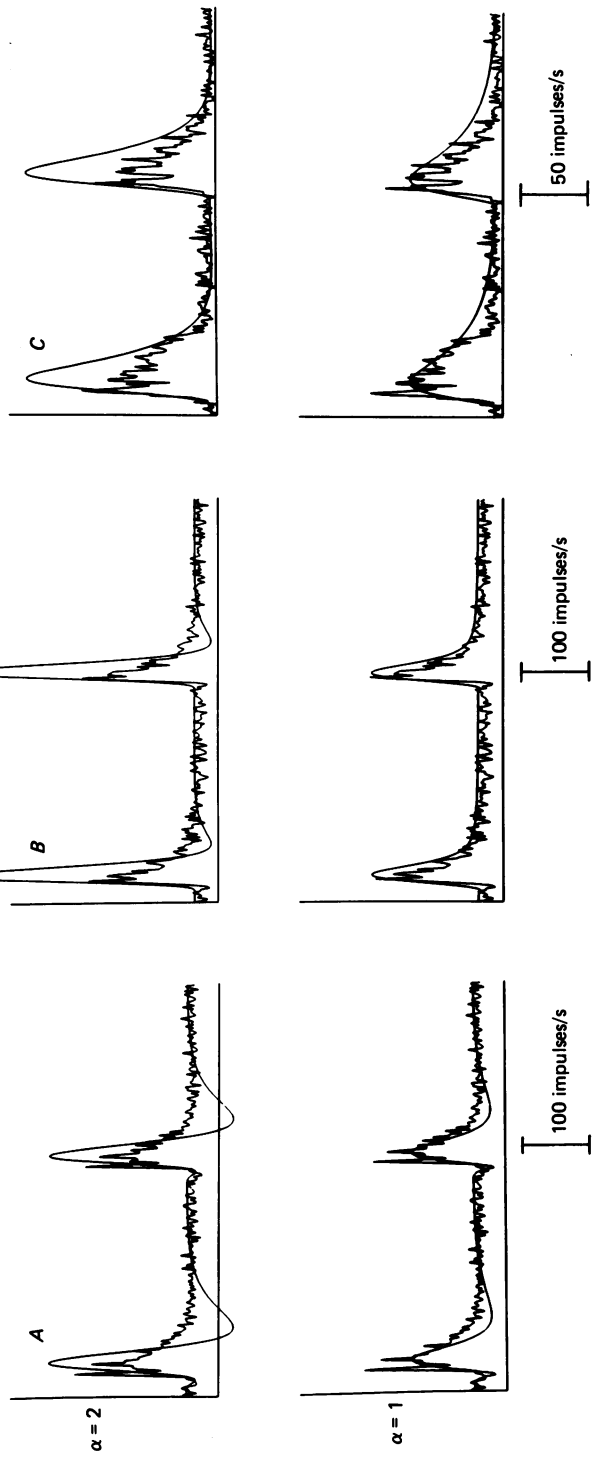

Fig. 4. Comparison of predicted and observed responses of Y ganglion cells to contrast reversal of a spatial sine grating. The irregular traces are response histograms elicited by 1·05 Hz square-wave contrast reversal of the grating at a modulation depth of $m_{syn} = 0{\cdot}5$. The smooth curves are predictions of the square-wave response derived from the model second-order frequency kernel and the model of Fig. 3 and Table 1, with parameters measured from the sum-of-sines stimulus with $m_{sns} = 0{\cdot}125$. In each panel, the prediction of the quadratic ($\alpha = 2$) model is on the top; the prediction of the rectifier ($\alpha = 1$) model is on the bottom. *A*, on-centre cell (of Figs 1 and 2) stimulated by a 2·0 cycles/deg grating; parameters as given in Fig. 2 *B*. *B*, on-centre unit 28/6 stimulated by a 1·5 cycles/deg grating. Parameters: $M_0 = 34{\cdot}0$, $A_0 b_2(\alpha) = 1526$, $N_{L,U} = 8$, $N_{L,U} T_{L,U} = 41{\cdot}8$ ms, $H_{s,U} = 0{\cdot}963$, $T_{s,U} = 0{\cdot}069$ s, $N_{L,w} = 8$, $N_{L,w} T_{L,w} = 11{\cdot}5$ ms, $H_{s,w} = 0{\cdot}717$, $T_{s,w} = 0{\cdot}016$ s, $D = 1$ ms. *C*, off-centre unit 23/2 stimulated by a 1·0 cycles/deg grating. Parameters: $M_0 = 3{\cdot}5$, $A_0 b_2(\alpha) = 207$, $N_{L,U} = 4$, $N_{L,U} T_{L,U} = 43{\cdot}9$ ms, $H_{s,U} = 1{\cdot}009$, $T_{s,U} = 0{\cdot}125$ s, $N_{L,w} = 12$, $N_{L,w} T_{L,w} = 11{\cdot}1$ ms, $H_{s,w} = 0{\cdot}237$, $T_{s,w} = 0{\cdot}101$ s, $D = 3$ ms.

reveal characteristics of the response not readily apparent from an order-by-order analysis.

The dynamical model is also tested by its ability to predict the response to a second sum-of-sinusoids signal. This sum-of-sinusoids signal, which is constructed on a denser frequency mesh, permits an experimental check of the extrapolation and interpolations implicit in the parametric model.

Square-wave responses. Figure 4 shows the responses of several Y cells to square-wave contrast-reversal of a sine grating. Superimposed on these response histograms are predictions generated by the linear–non-linear–linear sandwich model of Fig. 3. These model predictions were generated by successively applying the transformations of Table 1, with parameters extracted from the response to the sum-of-sinusoids signal as discussed above. The model parameter M_0, the mean rate in the absence of stimulation, was the impulse rate elicited by a uniform field of luminance equal to the mean stimulus luminance. For each response, the predictions of two models are shown: one assuming a quadratic non-linearity ($\alpha = 2$), one assuming a rectifying non-linearity ($\alpha = 1$).

For all of the eighteen cells whose second-order kernels were well described by the model eqn (10), the rectifier model provided very good agreement with the measured square-wave responses. The prediction of the quadratic non-linearity model, however, usually deviated substantially from the observed square-wave response, in that it overestimated the size of the transient response. This held both for on-centre cells (Fig. 4*A* and *B*) and off-centre cells (Fig. 4*C*). Furthermore, in the on-centre cells, the quadratic non-linearity model predicted a larger undershoot than was observed experimentally. Although this model has many parameters ($N_{L,U}$, $T_{L,U}$, $H_{S,U}$, $T_{S,U}$, $N_{L,W}$, $T_{L,W}$, $H_{S,W}$, $T_{S,W}$, A_0, α, M_0 and D), all but α have been determined without reference to the step responses: D was determined from retinal location, M_0 was the unstimulated mean firing rate, and the remaining parameters have been determined from 128 values (64 amplitudes and phases) of the second-order frequency kernel. The rectifier fit ($\alpha = 1$) is obviously not perfect; however, it is quite reasonable for a one-parameter fit.

It is worth emphasizing that the rectifier and quadratic models have identical second-order kernels at the contrast c_{ana}. The better fit of the rectifier model is essentially a consequence of the non-zero values of the higher-order kernels implicit in the rectifier non-linearity.

In comparing square-wave responses with model predictions, we have ignored the dependence of the Y cell non-linear dynamics on contrast (Shapley & Victor, 1980). As we will see below, this dependence has a relatively minor influence on the predicted square-wave response.

Responses to another sum-of-sines signal. A second test of the adequacy of the sandwich model was prediction of the response to a second sum-of-sines stimulus. This test was designed to check the interpolations and extrapolations implicit in the parametric forms (16) and (17), and to verify that the standard frequency set sampled the two-frequency interactions on a sufficiently dense mesh. The mesh of eight frequencies used in the sum-of-sinusoids signal (eqn (2)) for this experiment were: 1·352, 2·672, 4·454, 7·424, 9·338, 12·374, 16·202 and 20·624 Hz. These frequencies are exact integer multiples (41, 81, 135, 225, 283, 375, 491, 625) of the

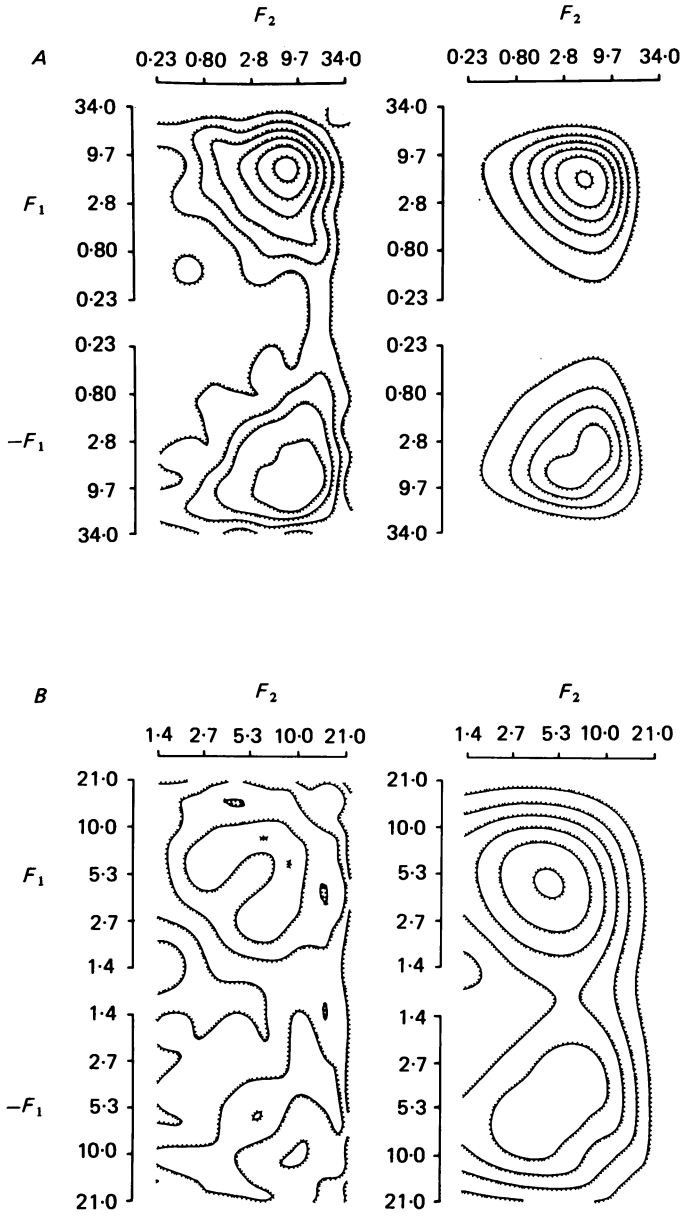

Fig. 5. Comparison of second-order frequency kernels measured with two sets of frequencies and sandwich model. *A*, left panel: kernel measured with standard frequency set, which was approximately equally spaced logarithmically from 0·231 to 33·758 Hz; right panel: model prediction. *B*, left panel: kernel measured with denser frequency set, which was approximately equally spaced logarithmically from 1·352 to 20·624 Hz; right panel: model prediction, derived from measured kernel of *A*. Off-centre unit 28/1; 0·75 cycles/deg grating; $m_{ana} = 0{\cdot}125$. In each case, measured and model kernels typically agree to within 1 impulse/sec. Model parameters: $M_0 = 10{\cdot}2$, $A_0 b_2(\alpha) = 1140$, $N_{L,U} = 12$, $N_{L,U} T_{L,U} = 54{\cdot}6$ ms, $H_{S,U} = 0{\cdot}958$, $T_{S,U} = 0{\cdot}066$ s, $N_{L,W} = 4$, $N_{L,W} T_{L,W} = 22{\cdot}6$ ms, $H_{S,W} = 0{\cdot}612$, $T_{S,W} = 0{\cdot}012$ s, $D = 3$ ms.

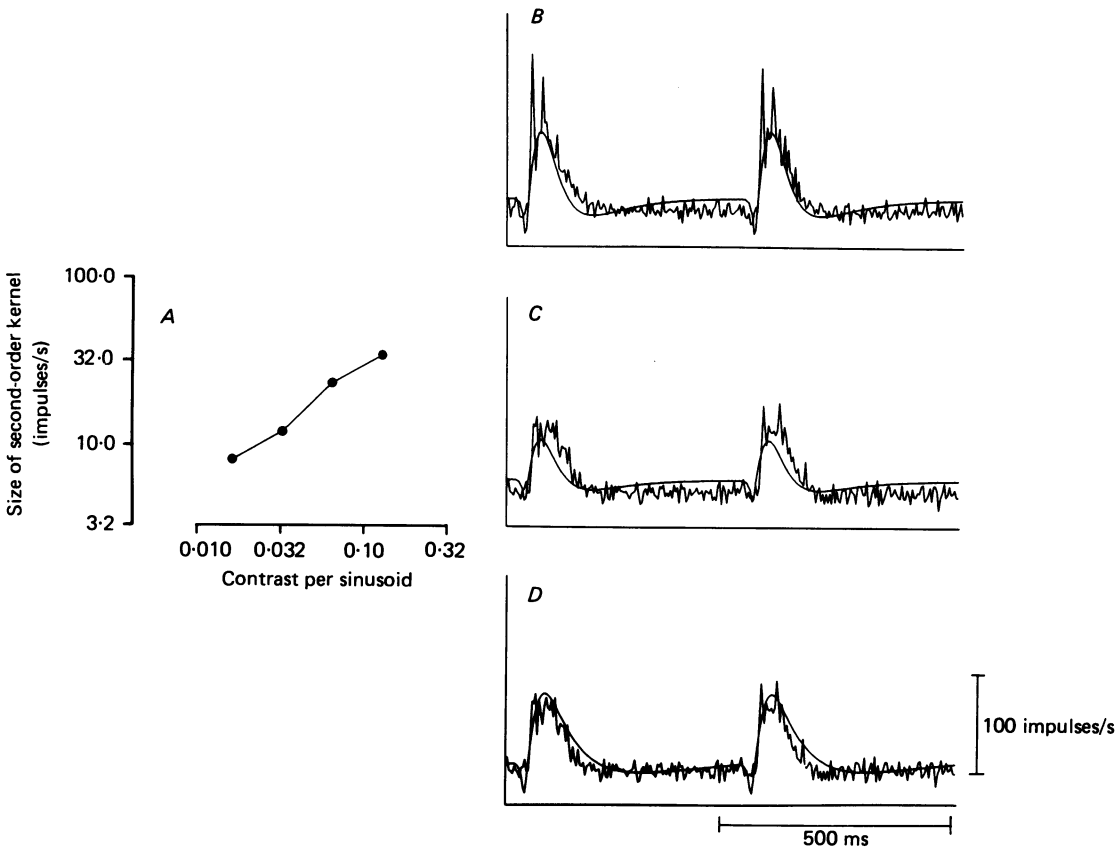

Fig. 6. Dependence of Y cell responses on contrast. *A*, dependence of the overall size of the second-order frequency kernel (measured as the square root of the sum of the squares of all the measured values of $K_2(\pm f_j, f_k; m_{ana})$ (eqn (6)) on analysis modulation depth m_{ana}. On logarithmic co-ordinates, the slope of the best-fitting line is 0·72, suggesting a power $\alpha = 0{\cdot}72$ for the non-linearity. *B*, comparison of the sandwich model prediction of the response to a square-wave stimulus with measured response ($m_{syn} = 0{\cdot}5$). The predicted response is calculated from parameters measured at a modulation depth of $m_{ana} = 0{\cdot}125$. Parameters are as in Fig. 2*B*, with $\alpha = 0{\cdot}72$. *C*, comparison of this sandwich model prediction with the measured response elicited by a square-wave stimulus at a lower modulation depth ($m_{syn} = 0{\cdot}25$). The dynamical parameters measured at $m_{ana} = 0{\cdot}125$ (*B*) are used, with $\alpha = 0{\cdot}72$. *D*, comparison of sandwich model prediction to the square-wave stimulus ($m_{syn} = 0{\cdot}25$), but using high-pass time constants $T_{S,U} = 0{\cdot}131$ s and $T_{S,W} = 0{\cdot}075$ s, as measured at a modulation depth $m_{ana} = 0{\cdot}0625$. Unit 7/6.

common fundamental frequency 0·032999 Hz. A phase algorithm analogous to the one used for the standard frequency set was employed to ensure freedom from overlaps of even-order components below order 8. As seen in Fig. 5, the experimentally measured second-order frequency kernel at this denser set of frequencies corresponded closely with that predicted from the sandwich model (eqn (10)) and parametric models (eqns (16) and (17)) for the linear filters U and W.

Dependence on contrast

In X cells, responses at higher contrasts are more transient than responses at lower contrasts (Shapley & Victor, 1978, 1981). For centre responses, this modulatory effect of contrast can be understood as a dynamic adjustment of the high-pass time constant: at higher contrasts, this time constant is shorter, and the response is more transient. An analogous modulation of the non-linear response of Y cells has previously been reported (Shapley & Victor, 1980). The parametric description of the Y cell non-linear response will allow us to examine the effect of contrast on the Y cell response in more detail, and to compare the effect of contrast on subunit dynamics with the effect of contrast on X cell centres.

If Y cell dynamics were independent of contrast, then eqn (10) (along with eqn (13)) would imply that the overall size of the second-order kernel is proportional to $(m_{\text{ana}})^{\alpha}$, and that its shape is independent of contrast. Since dynamics do in fact depend on modulation depth, there is a gentle change in shape of the second-order kernel with contrast. However, the overall size of the second-order kernel can still be used to approximate α. Then, the dependence of the shape of the second-order frequency kernel on contrast can be interpreted in terms of dependence of the dynamical parameters on contrast. This approach is analogous to the approach taken previously (Victor, 1987) for the analysis of the dependence of the first-order frequency kernels of X cells on contrast. Its application to non-linear transductions relies on the separation of linear and non-linear components of the cascade into independent factors in the sandwich model (eqn 10)).

The dependence of overall kernel size of one on-centre Y cell on input modulation depth m_{ana} is shown in Fig. 6*A*. Overall second-order kernel size grows proportionally to $(m_{\text{ana}})^{0.72}$. This suggests that $\alpha = 0.72$ is a more realistic characterization of the non-linearity (eqn (12)) than $\alpha = 1$. Similar analyses in the other Y cells yielded an average value of 0·87 for α (range, 0·71–1·01).

The dependence of the shape of the second-order frequency kernel on contrast may be summarized by the change in the values of the dynamical parameters measured at each contrast. In on-centre cells, reliable values for the dynamical parameters could be determined at the two or three highest modulation depths ($m_{\text{ana}} = 0.03125$, 0·0625 and 0·125 per sinusoid). Because off-centre responses were smaller, comparably reliable measurements could not be obtained at lower contrasts for these units.

The main systematic changes occurred in the high-pass time constants $T_{S,U}$ and $T_{S,W}$. The high-pass time constant of the first linear filter $T_{S,U}$ typically fell by a factor of 1·85 (geometric mean; range, 1·26–6·75) over the measureable range. The high-pass time constant of the second linear filter $T_{S,W}$ fell by a factor of 1·44 (geometric mean; range, 0·71–9·10) over this range. Changes in the low-pass time constants ($T_{L,U}$, $T_{L,W}$) were on the order of 20%; changes in the high-pass strengths ($H_{S,U}$, $H_{S,W}$) were on the order of 10%. These latter changes were inconsistent across units, and not analysed further.

As we have seen in Fig. 4, a large error in the exponent α of the non-linearity (i.e. $\alpha = 2$ instead of $\alpha = 1$) leads to large alterations in the predicted step response. However, smaller changes in the exponent have little effect on the predicted step

response. Step responses for an on-centre Y cell predicted from $\alpha = 1$ (Fig. 4*A*)) fit about as well as step responses predicted from the value $\alpha = 0{\cdot}72$ (Fig. 6*B*) deduced from the contrast dependence of the overall kernel size. This is because the main effect of the exponent α is to adjust the overall scaling of the response across contrasts. At any single contrast, changes in apparent gain A_0 can compensate for small errors in the value of α (see Appendix).

The effect of contrast-dependent adjustment in dynamics on the step response is shown in Fig. 6*C* and *D*. Here, the step response measured at $m_{\text{syn}} = 0{\cdot}25$ is compared with predictions made from two sandwich models. In Fig. 6*C*, the sandwich dynamics are derived from the kernel measured at $m_{\text{ana}} = 0{\cdot}125$; in Fig. 6*D*, the

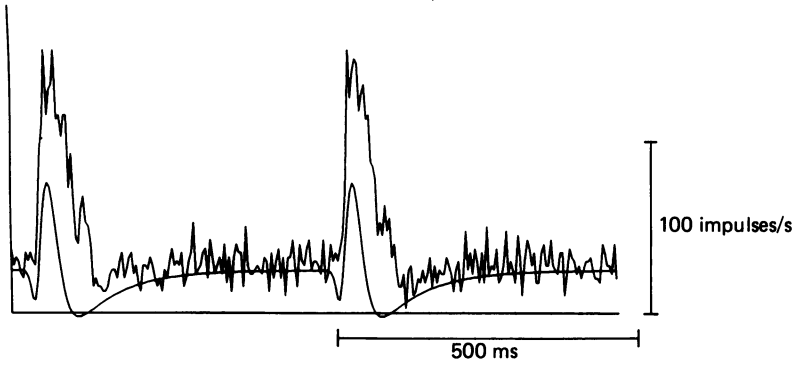

Fig. 7. Irregular curve: response to a square-wave stimulus of an on-centre Y cell which is not well fitted by the sandwich model. The stimulus was a 2·5 cycles/deg grating at a modulation depth $m_{\text{syn}} = 0{\cdot}25$. Smooth curve: prediction of the sandwich model. Parameters: $M_0 = 40{\cdot}7$, $A_0 b_2(\alpha) = 2128$, $N_{\text{L},U} = 8$, $N_{\text{L},U} T_{\text{L},U} = 33{\cdot}1$ ms, $H_{\text{S},U} = 0{\cdot}575$, $T_{\text{S},U} = 0{\cdot}072$ s, $N_{\text{L},W} = 8$, $N_{\text{L},W} T_{\text{L},W} = 16{\cdot}7$ ms, $H_{\text{S},W} = 1{\cdot}149$, $T_{\text{S},W} = 0{\cdot}009$ s, $D = 2$ ms. Unit 28/8.

dynamics are derived from the kernel measured at $m_{\text{ana}} = 0{\cdot}0625$. There is a twofold difference in the first filter's high-pass time constant $T_{\text{S},U}$, and more than a fourfold difference in the second filter's high-pass time constant $T_{\text{S},W}$ at these two contrast levels. These differences lead to a difference in the predicted step responses, but the difference is primarily a change in the overall response size. Thus, although the intensive characteristics of the non-linearity N and the dependence of the dynamical parameters on contrast may be extracted from the frequency-kernel data, this information is not apparent from the step responses.

Units not fitted well by the linear–non-linear–linear sandwich

For five of the twenty-three ganglion cells studied, it was not possible to determine model parameters which provided a reasonable fit to the observed second-order frequency kernel. The square-wave response of one such on-centre Y cell is shown in Fig. 7. This response appears similar to that of other Y cells which were well fitted by the procedures described above. The second-order frequency kernel of this unit is shown in Fig. 8*A*. One salient feature of this plot is the presence of a zero in the frequency kernel, located at approximate co-ordinates ($F_1 = -2$ Hz, $F_2 = 8$ Hz). In the neighbourhood of this point, the phase makes a complete circle about zero, as seen by the colouring of contour lines that circle this point. Phase is a continuous function

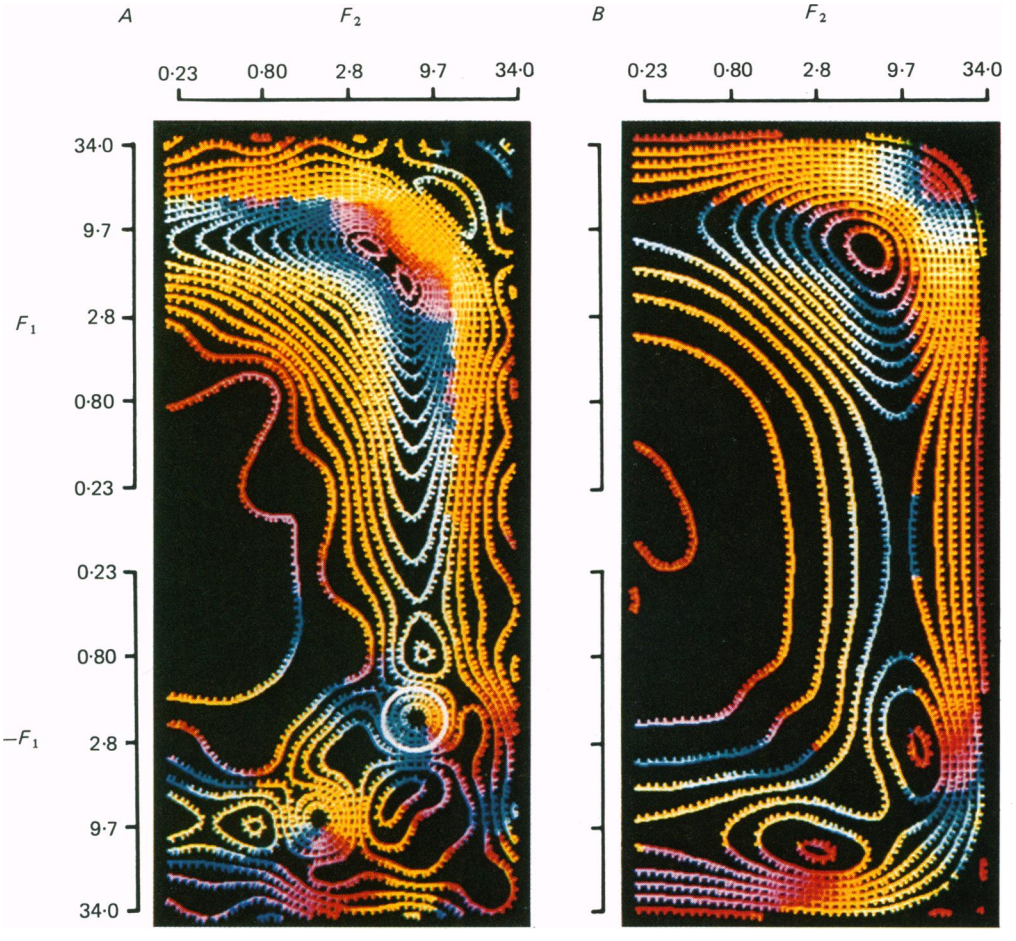

Fig. 8. *A*, second-order frequency kernel of a Y cell which was poorly fitted by the sandwich model (eqn (10)). The circle centred at co-ordinates ($F_1 = -2$ Hz, $F_2 = 8$ Hz) encloses a zero of the second-order kernel. *B*, best-fit parametric sandwich model to the measured second-order frequency kernel of *A*. Data is displayed as in Fig. 2. Unit 28/8.

of the value of the second-order frequency kernel except when the kernel has a value of zero (in which case, phase is indeterminate). Thus, these contour lines must enclose a point at which the second-order kernel has a value of zero.

This feature, the presence of an isolated zero, is inconsistent with the sandwich model for *any* choice of filter functions $\tilde{U}$ and $\tilde{W}$. To see this, observe that the second-order kernel of a linear–non-linear–linear sandwich (eqn (10)) is a product of three frequency-dependent terms. If the second-order kernel has a value of zero, then at least one of these terms [$(\tilde{U}(2\pi F_1)$, $\tilde{U}(2\pi F_2)$ or $\tilde{W}(2\pi(F_1+F_2))$] must be zero. This in turn would imply that the second-order frequency kernel was zero along a line of constant F_1, constant F_2, or constant F_1+F_2; this is inconsistent with the isolated zero implied by the data.

Thus, even the best-fitting sandwich model (Fig. 8*B*) provides a poor description

of the measured second-order frequency kernel, and leads to a poor prediction (Fig. 7) of the square-wave response. Alternative possibilities include additional serial non-linear stages of the cascade model, additional linear–non-linear–linear cascades in parallel, and dynamic contrast-dependent adjustment of the 'linear' stages of a single linear–non-linear–linear cascade. The analysis of the dependence on contrast suggests that dynamic contrast-dependent adjustment of the 'linear' stages does in fact occur (see above and Discussion); this is the simplest explanation for the observed isolated zeroes. Numerical simulations indicate that additional serial non-linear stages would not generate isolated zeroes robustly, but the possible role of additional parallel cascades cannot be excluded.

DISCUSSION

Summary of the model

The proposed dynamical model (Table 1 and Fig. 3) is a formalization of the linear–non-linear–linear sandwich previously introduced (Victor & Shapley, 1979), to which specific functional forms for the linear transductions of the model have been added.

The first stage of the model ('U' in Fig. 3) has as its input retinal luminance $L(X, Y, t)$. A preliminary transformation extracts the signed Weber fraction $s(t)$ from the input luminance. The output of the first linear stage, $u(t)$, is a linear transformation of luminance fluctuation, $s(t)$. The transformation from $s(t)$ to $u(t)$, given by eqns (7) and (16), represents linear processing within the subunit.

The non-linearity of the subunit is represented by a power-law transformation (eqn (12)), with exponent α approximately 0·87. This transformation produces the subunit output signal, $u'(t)$. The spatial combination of subunit outputs $u'(t)$ to produce a pooled signal $w(t)$ is represented by a linear transformation W, and is defined by eqns (9) and (17). The process of impulse generation is assumed to be linear, except for the addition of an undriven mean rate M_0 and the requirement for a non-negative firing rate. A brief conduction delay D, calculated from the Y cell's retinal location from the data of Stone & Fukuda (1974), is included in order to allow direct comparison with experimental data.

The analysis of the Y cell non-linear response in terms of an initial stage of linear processing, followed by a static non-linearity, followed by a second linear stage, provides a mathematical dissection of the Y cell response. To illustrate the dissection of the 'typical' on- and off-centre Y cells, we have displayed the results of each stage of the transduction in Fig. 9. The main features of this dissection are the effects of the non-linearity and the second linear stage on the shape of the subunit response.

Integration into a spatiotemporal model. Although this model is presented as a temporal model, it may be integrated readily into a *spatio*temporal model. Previous studies (Hochstein & Shapley, 1976*a*, *b*; Victor & Shapley, 1979) showed that the Y cell non-linear response to a sine grating is highly independent of the spatial phase of the grating. This implies that there are on the order of 100 non-linear subunits at random spatial positions. The outputs of these subunits combine to form one component of the Y cell response. At lower spatial frequencies, classical centre and surround mechanisms contribute as well.

Within each subunit, spatiotemporal coupling occurs: the subunit transduction (here denoted U) is shifted to higher temporal frequencies at lower spatial frequencies (p. 684 of Victor & Shapley, 1979). Further details of a spatiotemporal model, such as the spatial distribution of the subunits, cannot be specified on the basis of these studies.

A separate consideration is that the contrast-reversing gratings of high spatial frequency not only eliminate centre and surround contributions, but also eliminate any odd-order components that might be generated by the subunit itself. Thus, this analysis cannot distinguish between a full-wave rectifier $N(u) = |u|^{\alpha}$ and the corresponding half-wave rectifier whose output is zero for negative values of u. Half-wave rectification is the more plausible alternative physiologically (Toyoda, Hashimoto & Ohtsu, 1973; Naka, Marmarelis & Chan, 1975). However, the non-linear Y cell response cannot simply be a rectified centre response, because of its distinctive spatial characteristics.

Limitations of the model

The sandwich model implies that the dynamical parameters are independent of contrast. This is approximately true for the low-pass time constants ($T_{L,U}$, $T_{L,W}$) and the high-pass strengths ($H_{S,U}$, $H_{S,W}$). However, there is a systematic shortening of the values of the high-pass time constants $T_{S,U}$ and $T_{S,W}$ with increasing contrast. We interpret this dependence as a tuning of retinal dynamics driven by local contrast, which is analogous to the action of the contrast gain control on dynamics of X and Y cell centre responses (Shapley & Victor, 1979, 1980). In X cells, it was possible to determine the rate at which changes in the neural measure of contrast altered dynamics (Victor, 1987); in Y cells, greater uncertainty in determination of the dynamical parameters themselves precludes this determination.

Five of the twenty-three cells studied were not well fitted by the sandwich model (Figs 7 and 8). This failure cannot be a consequence of the particular functional forms (eqns (16) and (17)) postulated for the linear dynamics. The observed second-order frequency kernels of these five units had evidence of an isolated zero (Fig. 8), which would not be produced by any linear–non-linear–linear sandwich model.

Although the 'isolated zero' effectively rules out the linear–non-linear–linear model, it is unhelpful in suggesting an alternative. This is because a zero that occurs in a 'typical' second-order frequency kernel will, generically, be isolated. To see this, decompose the second-order kernel $K_2(f,g)$ into its real and imaginary parts:

$$K_2(f,g) = K_{\text{real}}(f,g) + \iota K_{\text{imag}}(f,g). \tag{19}$$

Assume that $K_2(f_0,g_0) = 0$. Near this point, real and imaginary parts of eqn (19) may be expanded as a Taylor series in the quantities $\Delta f = f - f_0$ and $\Delta g = g - g_0$:

$$\left.\begin{aligned} K_{\text{real}}(f,g) &\simeq \frac{\partial K_{\text{real}}}{\partial f}\Delta f + \frac{\partial K_{\text{real}}}{\partial g}\Delta g, \\ K_{\text{imag}}(f,g) &\simeq \frac{\partial K_{\text{imag}}}{\partial f}\Delta f + \frac{\partial K_{\text{imag}}}{\partial g}\Delta g. \end{aligned}\right\} \tag{20}$$

If the zero at (f_0, g_0) is *not* isolated, it must be possible to choose small increments Δf and Δg for which both real and imaginary parts of eqn (20) are equal to zero. This is only possible if the determinant,

$$\text{Det} = \frac{\partial K_{\text{real}}}{\partial f}\frac{\partial K_{\text{imag}}}{\partial g} - \frac{\partial K_{\text{real}}}{\partial g}\frac{\partial K_{\text{imag}}}{\partial f}, \tag{21}$$

is equal to zero. Since this determinant is composed of four independent real quantities, the generic situation is that it is *non*-zero, and the zero at (f_0, g_0) is isolated.

The approximation given by eqn (20) reveals that phase changes by a full cycle as an isolated zero is encircled. The direction of phase change is determined by the signature of the determinant (21).

Isolated zeroes such as those seen in Fig. 8 are thus found in a wide variety of non-linear systems, including parallel combinations of distinct linear–non-linear–linear sandwiches, multilayer sandwiches, and systems with non-linear feed-back.

There is much cell-to-cell variation in the strength of the contrast gain control, and it is likely that this phenomenon, rather than a distinctive qualitative feature of receptive-field structure, is responsible for the occasional failure of the sandwich model. The sandwich model is admittedly an approximation. The action of the contrast gain control on the filters U and W is modelled in a steady-state fashion: at each level of contrast, the basic sandwich eqn (10) is used, but the particular values of two time constants, $T_{S,U}$ and $T_{S,W}$, depend parametrically on contrast. The effects of dynamic adjustment of the filters U and W, due to changing levels of the neural contrast signal, are ignored in the present treatment. In X cells, the effects of the dynamic contrast gain control can be measured directly (Victor, 1985, 1987); the contrast gain control adjusts retinal dynamics rapidly (i.e. within 50 ms). Presumably, similarly rapid dynamics are present in the Y cell pathway as well, although direct confirmation of this is not possible with the present data. Rapid dynamic adjustment of the linear filters U and W introduces small corrections into the predicted second-order frequency kernel (eqn (10)), which are sufficient to produce the isolated zeroes for some values of the dynamical parameters.

On-centre and off-centre cells

We have shown (Figs 2–5) that for most Y cells, the parametrized sandwich model provides a reasonable description of subunit dynamics. We now use the model to examine the properties of on- and off-centre Y cells (Table 2), and to compare Y cell dynamics with X cell dynamics.

Although there is considerable variability of dynamical parameters across the sample studied (Table 2), some consistent differences between the on-centre and off-centre cells emerge. The total low-pass integration time of the initial linear filter, $N_{L,U}T_{L,U}$, is relatively constant within either the on-centre or off-centre cells, and is significantly longer in on-centre cells than in off-centre cells (47·9 ms *vs.* 36·8 ms, $P < 0{\cdot}05$). Conversely, the total low-pass integration time of the second linear filter, $N_{L,W}T_{L,W}$, is, on average, significantly shorter in on-centre cells than in off-centre cells (3·8 ms *vs.* 11·9 ms, $P < 0{\cdot}01$). The total low-pass integration time in on-

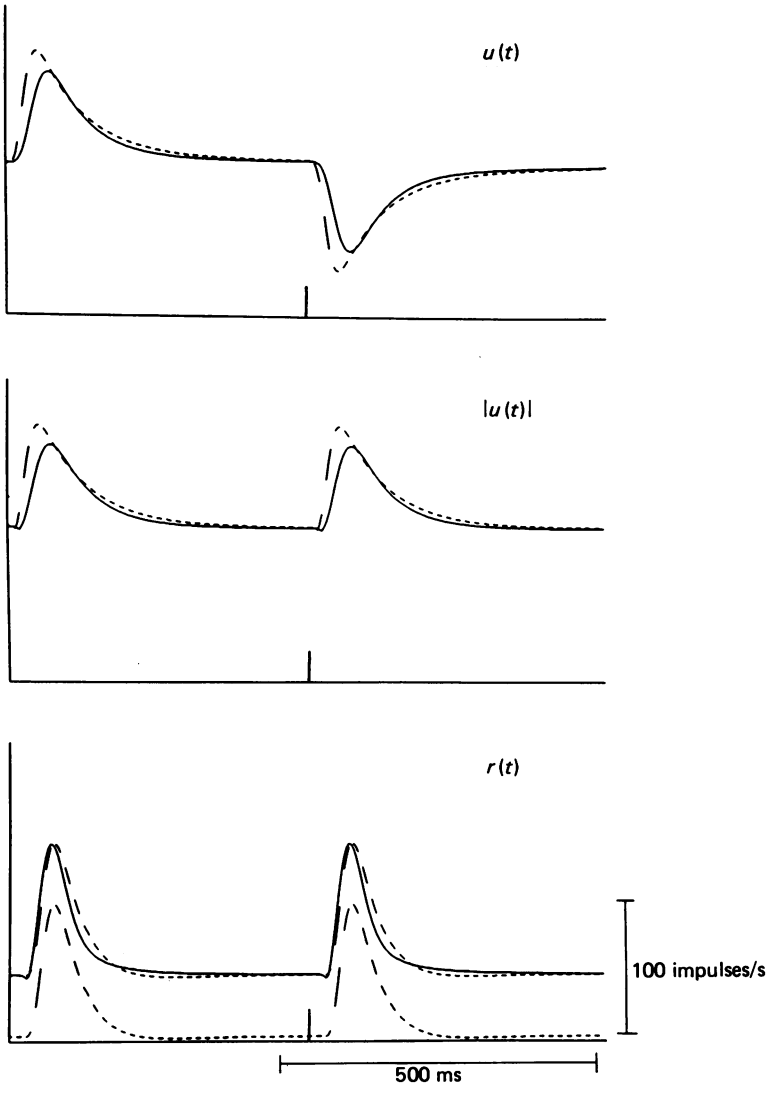

Fig. 9. Model responses, and theoretical curves for internal model variables, for 'typical' on-centre (continuous) and off-centre (dashed) Y cells stimulated by a square-wave reversing grating at a modulation depth of $m_{syn} = 0{\cdot}5$. Stimulus contrast reversal occurs at the beginning and mid-point of each graph, as indicated by the tickmarks. In the final panel, the off-centre unit's response $r(t)$ is plotted twice: once with the low mean rate observed in off-centre units, and once displaced upward to facilitate comparison with the on-centre unit's response. Parameters are the median values given in Table 2, with undriven firing rates $M_0 = 42{\cdot}7$ for the on-centre unit, and $M_0 = 2{\cdot}0$ for the off-centre unit.

and off-centre cells, $N_{L,U}T_{L,U}+N_{L,W}T_{L,W}$, is almost identical in both centre types (51·7 ms in on-centre cells, 48·7 ms in off-centre cells).

Although the low-pass components of on- and off-centre Y cells differ significantly, the high-pass parameters of the first linear filter are similar ($P > 0{\cdot}1$ for the high-pass

strength $H_{S,U}$ and the high-pass time constant $T_{S,U}$). There is considerable dispersion in the values of the high-pass time constants $T_{S,U}$ (coefficient of variation 0·9), so it is possible that a minor difference between the values in on- and off-cells would not be detected. However, despite a similar dispersion of values, there are clear differences between the dynamics of subunit pooling in on- and off-centre cells, as reflected in the parameters of the second high-pass stage. In on-centre Y cells, the

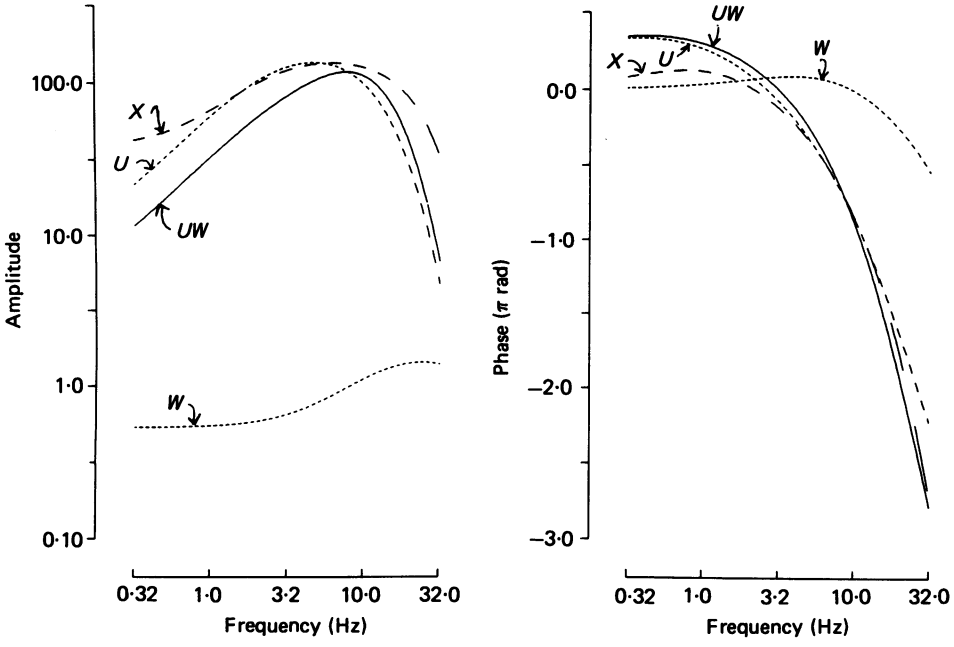

Fig. 10. A comparison of the transfer function of the 'typical' on-centre X cell centre with the model transfer functions of the 'typical' on-centre Y cell subunit. Long-dashed curve: effective transfer function of on-centre X cell; short-dashed curves: the model transfer functions $\tilde{U}(2\pi f)$ and $\tilde{W}(2\pi f)$; continuous curve: $\tilde{U}(2\pi f)\,\tilde{W}(2\pi f)$. The X cell data are from Victor (1987) with $c_{ana} = 0{\cdot}125$; the Y cell data are from Table 2 with gains assigned as described in the text.

high-pass strength $H_{S,W}$ is typically 50% stronger than in off-centre cells, and the time constant $T_{S,W}$ of this process is three or four times shorter.

The off-centre cells typically have an overall gain which is less than half that of the on-centre cells. However, the high-pass time constant $T_{S,W}$ is typically much longer in off-centre cells than in on-centre cells. At low temporal frequencies, these two differences have opposite effects: in comparison with on-centre cells, off-centre cells have a smaller attenuation due to the second linear filter W, but also have a smaller overall gain. The net effect is that the typical off-centre response transient is similar to the typical on-centre response transient (Fig. 9), even though the underlying dynamics are rather different.

For X cells, the smaller apparent gain and minor differences in dynamical parameters exhibited by the off-centre cells are, in large part, consequences of their lower firing rate (Victor, 1987). How much of the measured differences in gain and

dynamics between on- and off-centre Y cells might be due to the lower maintained firing rate of off-centre cells? For approximately linear transductions such as that of the X cell centre, this analysis was relatively straightforward: a spike-generating non-linearity, idealized as a transducer that truncates abruptly at zero impulses/s, had easily predictable effects on the first-order frequency kernel of an otherwise linear transduction. For the non-linearity of the Y cell subunit pathway, no such simplifying analytic results are available. Nevertheless, the effect of a lower firing rate on the apparent values of the dynamical parameters can be analysed empirically.

TABLE 3. The effect of firing rate on dynamical parameters

	Y on measured	Y on synthesized					Y off measured
		$M_0 = 42{\cdot}7$	$M_0 = 5$	$M_0 = 0$	$M_0 = -5$	$M_0 = -10$	
Parameter							
$A_0 b_2(\alpha)$ (impulses s^{-1} (unit contrast)$^{-2}$)	1305	1306	1275	1016	785	590	493
M (impulses/s)	51·5	51·5	14·3	10·1	6·8	4·3	12·3
$N_{L,U} T_{L,U}$ (ms)	49·4	49·7	49·0	46·3	43·8	41·5	31·9
$H_{S,U}$ (dimensionless)	0·964	0·963	0·962	0·961	0·961	0·962	0·958
$T_{S,U}$ (s)	0·056	0·054	0·050	0·048	0·047	0·046	0·074
$N_{L,W} T_{L,W}$ (ms)	8·6	7·8	8·0	8·9	10·0	11·2	22·6
$H_{S,W}$ (dimensionless)	0·717	0·681	0·619	0·513	0·412	0·337	0·554
$T_{S,W}$ (s)	0·011	0·014	0·013	0·015	0·018	0·018	0·046

Calculation of the effect of truncation on measured dynamical parameters. Column 1 contains the median on-centre Y cell parameters determined from thirteen units. The resulting model was then used to synthesize theoretical responses to the sum-of-sinusoids signal (eqn (2)), with the modulation depth per sinusoid $m_{ana} = 0{\cdot}125$. Truncation due to impulse generation was simulated by considering in sequence a range of postulated undriven firing rates M_0 (eqn (I) of Table 1); the firing rate was truncated to zero when the sum of the model response and M_0 was zero or less. These truncated impulse trains elicited by the sum-of-sinusoids signal were then used to extract model parameters, as described in the text. The second high-pass parameter $H_{S,W}$ was quite sensitive to this truncation; other parameters were insensitive to truncation. Truncation does not explain the difference in measured dynamics of the on-centre (column 1) and off-centre (column 7) units.

The strategy employed is to generate responses to the sum-of-sinusoids test signal from the typical dynamical parameters of on-centre cells, and then to truncate this response by assuming a range of hypothetical undriven firing rates M_0 (Table 1). The resulting *truncated* responses are then analysed by the above-described procedures for extraction of parameter values. Parameter values determined for artificial data generated from on-centre dynamical parameters but with M_0 near zero thus indicate the consequences of the truncation non-linearity alone.

The results of these calculations are shown in Table 3, for a test sum-of-sinusoids input with $m_{ana} = 0{\cdot}125$. An undriven firing rate M_0 of 42·7 impulses/s in the absence of stimulation produces a mean firing rate of 51·5 impulses/s with this standard input; this is the median firing rate of all on-centre Y cells. Parameters extracted from this resynthesized response (column 2 of Table 3) are essentially identical to the parameters used to generate the response (column 1). This is a check on the analytical procedure and the goodness of the approximation of eqn (10). In subsequent

calculations (columns 3–6 of Table 3), the undriven firing rate M_0 is lowered to a range which results in a stimulated mean firing rate typical of off-centre cells. An undriven firing rate M_0 of 0–5 impulses/s produces stimulated mean firing rates of in the range observed for off-centre cells (columns 3 and 4). But, this degree of truncation produces only a small decrement (less than 30%) in the apparent gain $A_0 b_2(\alpha)$, and not the two- or threefold difference observed (Table 2). Similarly, with the exception of the high-pass strength of the second linear filter $H_{S,W}$, the values of the other model parameters are affected only to a minor extent by this degree of truncation. The high-pass strength of the second linear filter $H_{S,W}$ is the one parameter whose apparent value is influenced by truncation. The size of the effect accounts for the apparently lower value of $H_{S,W}$ in off-centre cells. Thus, our analysis has shown that the lower gain, shorter $N_{L,U}T_{L,U}$, longer $N_{L,W}T_{L,W}$, and longer $T_{S,W}$ observed in off-centre Y cells as compared with on-centre Y cells all reflect intrinsic differences in the dynamics, and are not consequences of a lower maintained firing rate.

In sum, although the step responses of on- and off-centre Y cells are similar (Fig. 9), there is evidence that the subunit pathways have distinct internal dynamics. In off-centre Y cells, there is less temporal integration prior to rectification, and more integration following rectification, than in on-centre Y cells. It is now well established that the on- and off- channels of the centre pathway are anatomically separate at the level of the bipolar-to-ganglion cell connection (Nelson, Famiglietti & Kolb, 1978). Despite this anatomical on/off separation, no corresponding physiological difference appears to exist between the centre dynamics of on- and off-X cells (Victor, 1987). The present data indicate a physiological difference between subunits of on- and off-centre Y cells. Thus, the origin of the *physiological* difference between subunits of on- and off-centre Y cells probably resides in the inner plexiform layer.

Comparison with X cells

Previously, we have hypothesized that the bipolar cell, in addition to serving as the major linear input to the X cell, also corresponds to the Y cell subunit (Hochstein & Shapley, 1976*b*; Victor & Shapley, 1979). This hypothesis was based on the overall similarity of the spatial extent of Y cell subunits and X cell centres, and the qualitative similarity of X cell centre dynamics and Y cell non-linear subunit dynamics. More recently, Soodak, Shapley & Kaplan (1987) have demonstrated differences in the detailed spatial structure of X and Y cell centre mechanisms, which suggest differences in the spatial combination of bipolar signals between these two cell types. Their approach did not reveal a difference between X cell centres and Y cell non-linear subunits, perhaps because the multiplicity of Y cell subunits masked any signs of spatial fine structure. These considerations, in addition to the long-standing question of the relationship between the characteristics of transience and non-linearity, prompted a detailed comparison of X cell centre dynamics with those of the Y cell non-linear subunit dynamics.

The overall integration time in the Y cell non-linear pathway, $N_{L,U}T_{L,U} + N_{L,W}T_{L,W}$, averages 56·6 ms. This overall integration time is substantially longer than the integration time in the X cell linear pathway, which averages 32·8 ms

(Victor, 1987); no X cell in that sample had an integration time greater than 49·2 ms. While the subunit pathway of Y cells has a longer integration time than the centre pathway of X cells, the centre pathways of these two cell types have a similar integration time (Shapley & Victor, 1981).

The additional integration time in the Y cell non-linear pathway is probably due in part to additional synaptic delays involving the amacrine cells. Some, but not all, of this additional temporal integration may be ascribed to the linear filter W of the Y cell subunit pathway which follows the non-linearity; its integration time $N_{L,W}T_{L,W}$ averages 13·0 ms. The integration time of the first linear filter alone, $N_{L,U}$ $T_{L,U}$, averages 43·6 ms in Y cells (47·9 ms in on-centre units, 36·8 ms in off-centre units). This exceeds the X cell average of 32·8 ms; the difference must reflect additional integration time in the Y cell pathway *prior* to rectification.

In the present Y cell population, the average high-pass strength of the first linear filter $H_{S,U}$ is 0·96. This is higher than the average high-pass strength H_S of 0·70 in X cells, and no X cell had a high-pass strength greater than 0·80. The initial high-pass time constant $T_{S,U}$ has an average value of 0·082 s in Y cells, as measured at a modulation depth of 0·125 per sinusoid. In X cells, the average value of the high-pass time constant under these conditions is 0·201 s, as calculated from the data of Victor (1987). Thus, one contributor to the greater transience of the Y cell is a greater high-pass strength and a more rapid high-pass time constant within the subunit. If indeed X and Y cells share the same bipolar cell population but have distinct amacrine cell inputs (McGuire *et al.* 1984), there must be some additional high-pass transduction at the bipolar–amacrine synapse. In this regard, it is notable that H. Sakai & K. Naka (personal communication) have recently demonstrated differentiation, as well as rectification, in the transmission from bipolar cells to C-type amacrine cells in the catfish retina.

The dynamics of the X cell centre and the initial filter of the Y cell subunit both show a decrease in the high-pass time constant as contrast increases. Over the contrast range 0·03125–0·125 per sinusoid, $T_{S,U}$ falls by a factor of approximately 1·85; for typical X cell centres, T_S falls by a factor of 2·05 over this range (Victor, 1987). Thus, in comparison with the centre pathway of X cells, the initial filter of the Y cell subunit pathway has an integration time which is approximately 10 ms longer, is somewhat more differentiating, and has a contrast gain control of similar magnitude.

Although differences between the dynamics of X cell centres and the first filter of Y cell subunits are statistically significant, it must be emphasized that there is considerable overlap. Some Y cells, such as those of Fig. 4*A*, have initial high-pass parameters that fall within the range encountered in the X cell population. For this reason, we look to the remainder of the Y cell pathway for additional contributions to the transient nature of the response. An accelerating non-linearity, such as a square-law transduction, in principle could produce additional transience. However, the non-linearity is not accelerating: to a first approximation, it is a simple rectifier, and to a finer level of approximation, it is a compressive power law non-linearity (eqn (12)), with α approximately 0·87. Rectification *per se* does not produce increased transience (compare signal $u(t)$ with $|u(t)|$ in Fig. 9); compressive non-linearities decrease transience.

The comparison of the transfer functions of 'typical' on-centre X cells and Y cells at high spatial frequencies is presented graphically in Fig. 10. For the X cell data, the transfer function plotted corresponds to the median parameters of the on-centre X cells, as assayed with a sum-of-sinusoids signal whose contrast per sinusoid c_{ana} was 0·125 (Victor, 1987). For the Y cell data, we have used the median parameters of the transfer functions $\tilde{U}$ (eqn (16)) and $\tilde{W}$ (eqn (17)), as measured at a contrast per sinusoid c_{ana} of 0·125. The product $\tilde{U}\tilde{W}$ is the first-order response of the sandwich model to a modulated patch of light. Its gain is therefore determined by the shape of the non-linearity; we postulate (see above) that the non-linearity is a half-wave rectifier. Gains cannot be unambiguously assigned to the individual filters $\tilde{U}$ or $\tilde{W}$; we have therefore arbitrarily plotted $\tilde{U}$ so that its peak amplitude coincides with that of the X cell transduction, and adjusted $\tilde{W}$ accordingly. The delay D has been incorporated into the second transduction $\tilde{W}$; its only effect is a small additional phase lag.

The X cell transduction is similar to that of the filter U, which represents processing within the subunit, although U has somewhat greater attenuation at low temporal frequencies. This is in keeping with previous observations that the transduction within the subunit and the transduction of the X cell centre are similar (Victor & Shapley, 1979).

The second transduction ('W' of Figs 3 and 10) represents the dynamics of pooling of subunit signals, and is without analogy in X cells. In on-centre cells, this stage is almost a pure differentiator in the range 3–20 Hz. (In off-centre cells, as pointed out above, the apparent values of the parameters are affected by non-linearities of the spike-generating mechanism). Because of this second transduction, the product $\tilde{U}\tilde{W}$ (Fig. 10) has a greater low-frequency attenuation than $\tilde{U}$ alone, and is tuned to higher frequencies. Thus, the final stage of the Y cell subunit pathway, the pooling across subunits, plays a major role in generating the characteristic transient nature of the response. This pooling probably takes place in the amacrine cell layer, but is distinct from the non-linearity *per se*.

APPENDIX

Calculation of the Hermite expansion of a symmetric power-law rectifier

This appendix carries out the evaluation of the expansion of a power-law rectifier (eqn (12)) as an orthogonal sum of Hermite polynomials. The multiplier b_2 in the expression (10) for the second-order frequency kernel of a linear–static non-linear–linear sandwich corresponds to the second coefficient in this series. Higher-order coefficients b_n in the orthogonal expansion are the multipliers for the higher-order Wiener and frequency kernels of this transduction. In calculating the coefficients b_n, the orthogonal expansion must be carried out with respect to a Gaussian of power (variance) P equal to the power passed by the initial linear filter of the sandwich (P_U, eqn (11)). Further background on this calculation may be found in Victor & Knight (1979). General properties of the Hermite polynomials required for this calculation may be found in Abramowitz & Stegun (1964, chapter 22). (Note that the normalization convention of the Hermite polynomials used here differs from that of Abramowitz and Stegun, in that here, the leading term of each polynomial is taken to be unity.)

In general, the nth coefficient b_n in the Hermite expansion of $N(u)$ with respect to a Gaussian of variance P is given by

$$b_n = \frac{\int_{-\infty}^{\infty} N(u) H_n(u) \,\mathrm{Gau}\,(u, P)\,\mathrm{d}u}{\int_{-\infty}^{\infty} (H_n(u))^2 \,\mathrm{Gau}\,(u, P)\,\mathrm{d}u}, \tag{22}$$

where $\mathrm{Gau}\,(u, P)$ represents the Gaussian distribution of zero mean and variance P:

$$\mathrm{Gau}\,(u, P) = (2\pi P)^{\frac{1}{2}} \exp(-u^2/2P). \tag{23}$$

With the present convention for the Hermite polynomials, the denominator of eqn (22) is equal to $n!P^n$. We calculate the numerator integral in eqn (22) for the $n = 2$–case; the general term b_n may be evaluated by similar means. The second Hermite polynomial in the convention used in Victor & Knight (1979) (eqn (22) of that reference) is $H_2(u, P) = u^2 - P$. Substituting this and the definition of the power-law non-linearity (eqn (12)) into eqn (22) leads to an expression for the second coefficient $b_2(\alpha)$ in the Hermite expansion of a power-law non-linearity:

$$b_2(\alpha) = \frac{1}{2P^2} \int_{-\infty}^{\infty} |u|^{\alpha}(u^2 - P) \,\mathrm{Gau}\,(u, P)\,\mathrm{d}u. \tag{24}$$

Because the non-linearity is symmetric, the value of the integral over the range $(-\infty, \infty)$ is twice its value over the range $(0, \infty)$. This change allows removal of the absolute-value operation:

$$b_2(\alpha) = \frac{1}{P^2} \int_{0}^{\infty} u^{\alpha}(u^2 - P) \,\mathrm{Gau}\,(u, P)\,\mathrm{d}u. \tag{25}$$

Next, replace u by the dimensionless variable $v = u/\sqrt{P}$, and use the definition of the Gaussian (eqn (23)):

$$b_2(\alpha) = (2\pi)^{-\frac{1}{2}} P^{\alpha/2-1} \int_{0}^{\infty} v^{\alpha}(v^2 - 1) \exp(-v^2/2)\,\mathrm{d}v. \tag{26}$$

For $\alpha \geqslant 0$, this simplifies after integration by parts, with the grouping $(v^2 - 1) \exp(-v^2/2)\,\mathrm{d}v = -\mathrm{d}[v \exp(-v^2/2)]$:

$$b_2(\alpha) = \alpha(2\pi)^{-\frac{1}{2}} P^{\alpha/2-1} \int_{0}^{\infty} v^{\alpha} \exp(-v^2/2)\,\mathrm{d}v. \tag{27}$$

Finally, we substitute $t = v^2/2$ and $\mathrm{d}t = v\mathrm{d}v$ to obtain

$$b_2(\alpha) = \alpha(2\pi)^{-\frac{1}{2}} P^{\alpha/2-1} 2^{((\alpha-1)/2)} \int_{0}^{\infty} t^{(\alpha-1)/2} \exp(-t)\,\mathrm{d}t. \tag{28}$$

The result in the text, eqn (13), follows from the observation that the integral above defines the Γ-function.

Professors E. Kaplan, B. Knight and R. Shapley contributed many helpful suggestions at all stages of this work. D. Edwards, M. Conte, C. Reid and R. Soodak provided excellent technical assistance. This work was supported in part by grants EY188, EY1428, EY2439, EY6871 and NS877 from the United States National Institutes of Health, The Harry Frank Guggenheim Foundation, the Hartford Foundation and the McKnight Foundation. A portion of this work was presented at the 1986 meeting of the Association for Research in Vision and Ophthalmology, in Sarasota, Florida.

REFERENCES

ABRAMOWITZ, M. & STEGUN, I. A. (1964). *Handbook of Mathematical Functions*. National Bureau of Standards. Reprinted in 1970. New York: Dover.

BAYLOR, D. A. & HODGKIN, A. L. (1974). Changes in time scale and sensitivity in turtle photoreceptors. *Journal of Physiology* **242**, 729–758.

BOYCOTT, B. B. & WÄSSLE, H. (1974). The morphological types of ganglion cells of the domestic cat's retina. *Journal of Physiology* **240**, 397–419.

CLELAND, B. G., DUBIN, M. W. & LEVICK, W. R. (1971). Sustained and transient neurones in the cat's retina and lateral geniculate nucleus. *Journal of Physiology* **217**, 473–496.

EFRON, B. (1980). *The jacknife, the bootstrap, and other resampling plans*. Technical report No. 63. Division of Biostatistics, Stanford University, Stanford, CA, U.S.A.

ENROTH-CUGELL, C. & ROBSON, J. G. (1966). The contrast sensitivity of retinal ganglion cells of the cat. *Journal of Physiology* **187**, 517–552.

FLETCHER, R. & POWELL, M. J. D. (1963). A rapid descent method for minimization. *Computer Journal* **6**, 163–168.

HOCHSTEIN, S. & SHAPLEY, R. M. (1976*a*). Quantitative analysis of retinal ganglion cell classifications. *Journal of Physiology* **262**, 237–264.

HOCHSTEIN, S. & SHAPLEY, R. M. (1976*b*) Linear and non-linear spatial subunits in Y cat retinal ganglion cells. *Journal of Physiology* **262**, 265–284.

KAPLAN, E. & SHAPLEY, R. M. (1984). The origin of the S (slow) potential in the mammalian lateral geniculate nucleus. *Experimental Brain Research* **55**, 111–116.

KORENBERG, M. J. (1973). Cross-correlation analysis of neural cascades. *Proceedings of the 10th Annual Rocky Mountain Bioengineering Symposium*, 47–51.

LENNIE, P. (1980). Parallel visual pathways: a review. *Vision Research* **20**, 561–594.

MCGUIRE, B. A., STEVENS, J. K. & STERLING, P. (1984). Microcircuitry of bipolar cells in cat retina. *Journal of Neuroscience* **4**, 2920–2938.

MILKMAN, N., SCHICK, G., ROSSETTO, M., RATLIFF, F., SHAPLEY, R. & VICTOR, J. (1980). A two-dimensional computer-controlled visual stimulator. *Behavioral Research Methods and Instrumentation* **12**, 283–292.

NAKA, K.-I., MARMARELIS, P. Z. & CHAN, R. (1975). Morphological and functional identification of catfish retinal neurons. III. Functional identification. *Journal of Neurophysiology* **38**, 92–131.

NELSON, R., FAMIGLIETTI, E. V. & KOLB, H. (1978). Intracellular staining reveals different levels of stratification for on- and off-center ganglion cells in the cat retina. *Journal of Neurophysiology* **41**, 472–483.

SHAPLEY, R. M. & VICTOR, J. D. (1978). The effect of contrast on the transfer properties of cat retinal ganglion cells. *Journal of Physiology* **285**, 275–298.

SHAPLEY, R. M. & VICTOR, J. D. (1980). The effect of contrast on the non-linear response of the Y cell. *Journal of Physiology* **302**, 535–547.

SHAPLEY, R. M. & VICTOR, J. D. (1981). How the contrast gain control modifies the frequency response of cat retinal ganglion cells. *Journal of Physiology* **318**, 161–179.

SOODAK, R., SHAPLEY, R. M. & KAPLAN, E. (1987). The subunit structure of receptive field centers of X and Y cells of the cat. *Journal of Neurophysiology* (in the Press).

STONE, J. & FUKUDA, Y. (1974). Properties of cat retinal ganglion cells: A comparison of W cells with X and Y cells. *Journal of Neurophysiology* **37**, 722–748.

TOYODA, J.-I., HASHIMOTO, H. & OHTSU, K. (1973). Bipolar–amacrine transmission in the carp retina. *Vision Research* **13**, 295–307.

VICTOR, J. D. (1985). The non-linear dynamics of the center mechanism of cat retinal ganglion cells. *Proceedings of the IEEE International Conference on Systems, Man, and Cybernetics. Tucson, Arizona*, 867–873.

VICTOR, J. D. (1987). The dynamics of the cat retinal X cell centre. *Journal of Physiology* **386**, 219–246.

VICTOR, J. D. & KNIGHT, B. W. (1979). Nonlinear analysis with an arbitrary stimulus ensemble. *Quarterly of Applied Mathematics* **37**, 113–136.

VICTOR, J. D. & SHAPLEY, R. M. (1979). The nonlinear pathway of Y ganglion cells in the cat retina. *Journal of General Physiology* **74**, 671–689.

VICTOR, J. D. & SHAPLEY, R. M. (1980). A method of nonlinear analysis in the frequency domain. *Biophysical Journal* **29**, 459–484.